EFFICIENT MOMENT METHOD AND HYBRID MOMENT METHOD SOLUTIONS FOR THE EM SCATTERING BY A DIELECTRIC LOADED RECTANGULAR CAVITY IN A GROUND PLANE

James R. Lyons
Prabhakar H. Pathak

The Ohio State University
ElectroScience Laboratory
Department of Electrical Engineering
Columbus, Ohio 43212

Technical Report 716611-1
Contract No. F33615-84-K-1550
July 1987

USAF/AFSC
Aeronautical Systems Division
Wright Patterson AFB, Ohio 45433

NOTICES

When Government drawings, specifications, or other data are used for any purpose other than in connection with a definitely related Government procurement operation, the United States Government thereby incurs no responsibility nor any obligation whatsoever, and the fact that the Government may have formulated, furnished, or in any way supplied the said drawings, specifications, or other data, is not to be regarded by implication or otherwise as in any manner licensing the holder or any other person or corporation, or conveying any rights or permission to manufacture, use, or sell any patented invention that may in any way be related thereto.

50272-101

REPORT DOCUMENTATION PAGE	1. REPORT NO.	2.	3. Recipient's Accession No

4. Title and Subtitle EFFICIENT MOMENT METHOD AND HYBRID MOMENT METHOD SOLUTIONS FOR THE EM SCATTERING BY A DIELECTRIC LOADED RECTANGULAR CAVITY IN A GROUND PLANE

5. Report Date July 1987

6.

7. Author(s) James R. Lyons and Prabhakar H. Pathak

8. Performing Organization Rept. No 716611-1

9. Performing Organization Name and Address
The Ohio State University ElectroScience Laboratory
1320 Kinnear Road
Columbus, Ohio 43212

10. Project/Task/Work Unit No

11. Contract(C) or Grant(G) No
(C) F33615-84-K-1550
(G)

12. Sponsoring Organization Name and Address
USAF/AFSC
Aeronautical Systems Division
Wright Patterson AFB, Ohio 45433

13. Type of Report & Period Covered
Technical

14.

15. Supplementary Notes

16. Abstract (Limit 200 words)

Two efficient moment method (MM) solutions are developed for the electromagnetic scattering by a two-dimensional rectangular cavity recessed in a perfectly-conducting ground plane and loaded with a homogeneous lossy or lossless dielectric. The unknown to be found in this MM solution is only the aperture electric field because of the use of special Green's functions for a conducting half-space and a fully closed conducting rectangular cavity. Both the TE and TM polarizations are treated. One MM solution employs a waveguide modal basis or expansion functions to represent the unknown aperture electric field and yields a solution which is efficient for narrow to moderately wide (<25 wavelengths) cavities of arbitrary depth. The use of an alternative form of the cavity Green's function further adds to the efficiency. The second MM solution uses a hybrid set of basis functions dictated by the physics of the problem; this hybrid solution is very efficient for treating wide and shallow cavities. Furthermore, the number of hybrid basis functions remain nearly a constant (about 10 or less) no matter how wide the cavity gets. Numerical results are shown to establish confidence in both approaches by comparing them with each other and with a conventional MM solution using pulse basis. This work is of interest in the scattering by antenna cavities.

17. Document Analysis a. Descriptors

b. Identifiers/Open-Ended Terms

c. COSATI Field/Group

18. Availability Statement	19. Security Class (This Report)	21. No of Pages
Approved for public release; distribution is unlimited.	Unclassified	107
	20. Security Class (This Page) Unclassified	22. Price

TABLE OF CONTENTS

LIST OF TABLES

LIST OF FIGURES

I. INTRODUCTION

A. THE PROBLEM

An efficient procedure is developed in this report for analyzing scattering of an electromagnetic-plane wave from a homogeneously loaded rectangular cavity recessed in a perfectly conducting ground plane. The analysis is performed for the two-dimensional geometry shown in Figure 1.1. The interest in this work stems in large part from the significant radar cross section (RCS) contribution of such geometries. Of special interest are loaded and unloaded notch geometries, in which the width and depth of the rectangular cavity are small to moderately large in terms of the wavelength, and also wide shallow cavities in which the

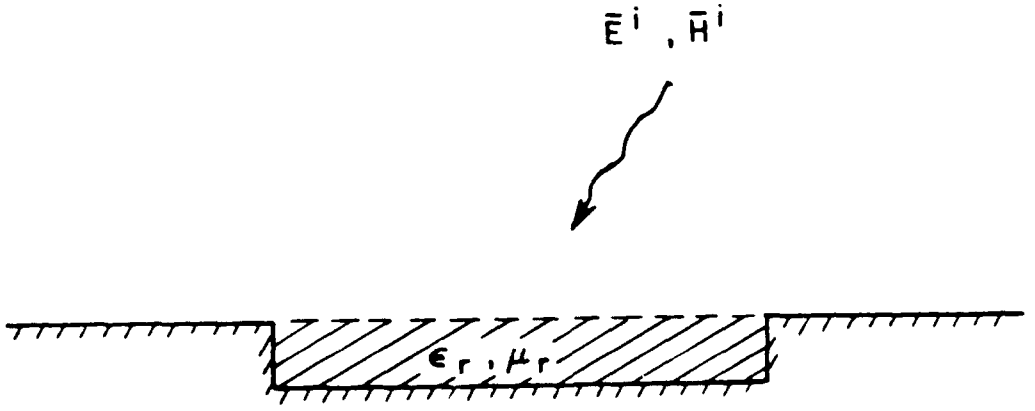

Figure 1.1. Electromagnetic fields incident on a loaded cavity recessed in a ground plane.

width of the cavity is large in terms of the wavelength while the depth is a fraction of a wavelength. The latter geometry is of particular interest because of its its application to surface wave antennas, and to arrays of dielectric covered slots.

The notch geometry is analyzed by a conventional numerical moment method technique cast into a particular efficient form. The wide shallow cavity, because of its large electrical size, cannot be efficiently analyzed by the same technique. Thus, a hybrid version of the moment method is developed for this geometry which results in a considerable savings of CPU time compared to the conventional moment method.

B. PREVIOUS RESEARCH

We consider first some previous work done on problems related to the scattering of a plane wave from 2-D dielectric loaded notch geometries. In each of these solutions the moment method [1] was employed to solve an integral equation involving the equivalent magnetic current in the aperture. Because of the relatively small electrical size of the notches conventional moment method techniques were used. Richmond [2] solved the problem of a dielectric loaded notch recessed in a perfectly conducting circular cylinder by expanding the fields in the dielectric in a set of cylindrical modes and then applying Galerkin's method to determine the aperture fields. Kautz, Pathak and Peters [3], as well as Wang [4] considered the geometry of a dielectric loaded gap

in a thick perfectly conducting screen. They determined the equivalent magnetic current (in both the upper and lower apertures) by employing the moment method in conjunction with the multiple scattering method. By placing an impedance wall in the lower aperture and assigning to it an impedance of zero, they are able to treat a loaded notch geometry. However, this method of solution for the notch problem is not very efficient, primarily because of the added complexity resulting from the formulation which allows one to treat the more general case of loaded gaps in thick screens.

We now consider some relevant previous research done on problems related to loaded wide shallow cavities. Pathak and Kouyoumjian [5] solved the canonical problem of surface wave diffraction by a truncated dielectric slab recessed in a perfectly conducting gound plane. They restricted their analysis to a lossless dielectric slab able to support only the TM_0 surface wave. The reflected and diffracted fields are expressed in terms of the geometrical theory of diffraction (GTD) [6]. The surface wave reflection and diffraction coefficients are obtained from a formally exact solution employing a combination of the generalized scattering matrix technique (GSMT) [7] and the Wiener-Hopf procedure [8]. This solution, although formally exact, requires considerable computation. A more efficient solution, which can also handle a discretely inhomogeneous portion of dielectric near the truncation, is given by Chuang [9]. This solution employs a moment method solution to an integral equation involving the equivalent magnetic current at the air-dielectric interface. Because of the

semi-infinite geometry, it is necessary to use a hybrid moment method [10], [11] solution in which the basis functions are pulses near the truncation and in the inhomogeneous portion of the dielectric; whereas, away from the truncation and inhomogeneous regions, the unknown surface field is expressed in terms of the incident and reflected surface waves together with the diffracted wave (which vanishes to first order on the dielectric interface). The forms of the reflected and diffracted waves are known and their amplitudes constitute unknowns to be determined. We can use this solution in conjunction with reciprocity to determine the lauching coefficient of a surface wave due to a plane wave incident on the canonical geometry. However, in this situation, reciprocity will not yield any information on the surface transition region which extends a couple of wavelengths (and even farther for a plane wave incident at grazing angles) from the truncation. This, coupled with the fact that the semi-infinite portion of dielectric must be lossless, limits the usefulness of that canonical problem in obtaining a solution to the problem shown in Figure 1.1. In addition, the solutions of Pathak, et al. and Chuang are only for an incident TM_0 surface wave; the other polarization is not treated, simply because the TE_1 surface wave is cutoff for the configuration considered by Pathak, et al. in [5].

Another solution relevant to the loaded shallow cavity problem is given by Richmond [12] for scattering of a plane wave from thin dielectric strips of infinite length; the electric field is parallel to the edges of the strip. The field in the dielectric is expanded in a sum of forced wave and two surface waves, with the amplitudes of these

waves being determined by Galerkin's method. This solution is relevant to the loaded shallow cavity problem because of the physical nature of the basis functions. However, the presence of the perfectly conducting surface in the case of the shallow cavity yields diffraction effects that are significantly different from the diffraction characteristics of the dielectric strip.

Finally, we mention a hybrid moment method solution to a problem not related to that being considered in this report, but which well illustrates the computational capabilities of the technique. Srikanth, Pathak, and Chuang [13] employed a hybrid uniform theory of diffraction (UTD) [14], [15], -moment method (MM) solution to analyze the plane wave scattering from an infinite, perfectly conducting semi-circular cylinder. A mixed basis expansion involving pulses near the edges and UTD functions elsewhere is used for the unknown current on the cylinder. The basis function amplitudes are then determined by point-matching. Numerical results show excellent agreement with conventional pulse basis expansions, and are obtained in a fraction of the CPU time of the latter method. We point out, however, that the hybrid UTD-MM is most applicable to a particular geometry when the diffraction characteristics (i.e., UTD diffraction effects) of the canonical features of that geometry are well understood.

In this thesis an efficient conventional moment method solution is presented for the scattering of a plane wave from a notch geometry and a very efficient hybrid moment method solution is presented for the special case of loaded wide shallow cavity. For the notch problem the

equivalent magnetic current in the aperture is expanded in a set of parallel-plate waveguide modes in which each mode is an entire domain basis function across the aperture. The unknown field is only over the extent of the aperture because the Green's function chosen in the formulation of the integral equation for the unknown in this geometry is comprised of two terms, one for a half-space with a perfectly conducting ground plane, and the other for a loaded, fully-enclosed, perfectly conducting cavity. Galerkin's method is used to determine the mode amplitudes. Only 3-4 modes per free-space wavelength are needed for a converged solution, as compared to the 10-20 pulses or piecewise sinusoids per wavelength that are usually necessary if subsectional basis functions were used. By using an appropriate form of the cavity Green's function, the cavity contribution to an individual impedance matrix element is arranged into a closed-form term plus a highly convergent summation. In fact, when using the waveguide mode basis functions, the closed-form contribution alone suffices. This, in addition to an evaluation of the half-space contribution employed by Richmond [12], yields a very efficient matrix fill. Excellent agreement has been found between the modal basis expansion presented here and a standard pulse basis solution. In addition, the modal basis solution was observed to be several times faster than the pulse basis solution. Practically speaking, the modal basis solution represents a cost-effective solution (on a VAX 11/780) to scattering from recessed rectangular cavities of width $\lesssim$ 25 wavelengths and of arbitrary depth.

Because of the special interest in dielectric covered antenna cavities, a separate solution was performed for the wide and shallow loaded cavity geometry. By 'wide and shallow' it is meant that the cavity width is greater than several wavelengths and the cavity depth and loading are such that at most only one surface wave mode exists. The same integral equation and Green's functions are used as for the previous discussion, but a different set of basis functions is employed. In this hybrid moment method solution the equivalent magnetic current in the cavity aperture is expanded as a forced wave and two surface waves (as in [12]) plus several additional basis functions that describe transition effects which are most significant near the cavity edges. Again, Galerkin's method is employed, but now the number of unknowns remains almost constant ($\lesssim 10$) regardless of the cavity width. Because the transition effects are described via a choice of exponential functions, the computation of the impedance matrix is not significantly different from that of the modal basis solution. The result is an extremely efficient solution for the wide and shallow loaded cavity. Good backscatter results have been obtained for the magnetic field parallel to the cavity edges for which case the TM_0 surface wave always exists, and when the cavity depth is nearly equal to or less than 0.1 wavelengths. For the other polarization, i.e., when the electric field parallel to the cavity edges, the lack of a surface wave mode in the dielectric for shallow cavities causes the hybrid moment method solution to be less accurate at grazing angles than the corresponding solution for the TM polarization. For both polarizations the hybrid basis

solution is far more computationally efficient for wide apertures than is the modal basis solution.

C. FORMAT

In Chapter II, the integral equations involving the equivalent magnetic current in the aperture are derived. In Chapter III, the moment method solution to the integral equations is described. In Chapter IV, numerical results for specific examples are presented and discussed. In Chapter V, the conclusions are stated.

A time convention of $\exp(j\omega t)$ is assumed and suppressed; only here does t refer to time.

II. INTEGRAL EQUATIONS FOR THE APERTURE FIELDS

A. LOADED CAVITY RECESSED IN A PERFECTLY CONDUCTING GROUND PLANE

Consider electromagnetic fields incident on the 2-D geometry shown in Figure 2.1. The source of the incident fields is assumed to be in region I as shown in the figure. The material in region II is assumed to be linear, homcgeneous, isotropic and time-invariant and may be either lossy or lossless. The problem considered here is the determination of the fields scattered in region I due to a known source which is also in region I.

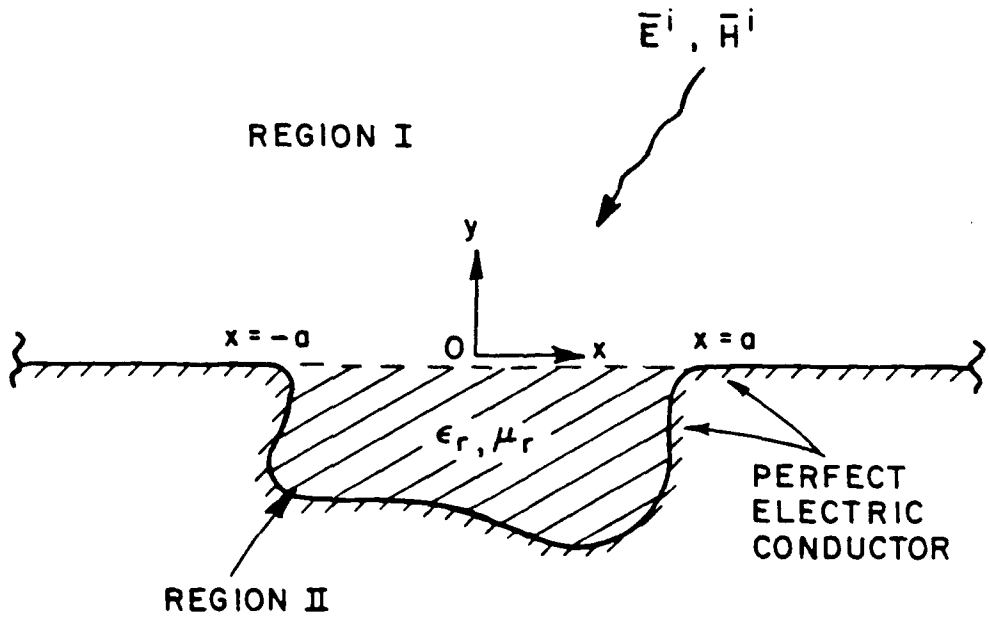

Figure 2.1. An arbtrary loaded cavity recessed in a perfectly conducting ground plane.

Since the geometry is 2-D, the general vector problem can be easily reduced to 2 scalar problems. The incident fields may be decomposed into 2 polarizations: (1) the electric field vector parallel to the conducting edge, denoted as the 'soft polarization' (subscript 's') case, and (2) the magnetic field vector parallel to the conducting edge, denoted as the 'hard polarization' (subscript 'h') case. Thus, we define the total scalar fields to be

$$u_{\substack{s \\ h}}(x,y) = \begin{vmatrix} E_z(x,y) \\ H_z(x,y) \end{vmatrix} \quad . \tag{2.1}$$

Integral equations, in which the unknown happens to be the electric fields only within the aperture at y=0 and $|x| < a$, may be derived in a straight-forward manner by the application of Green's second identity [16]. The details of this derivation are deferred to Appendix A; here we present only the resulting equations and their interpretation in terms of the equivalence principle. These integral equations are later solved by a moment method procedure [1] using a special set of only a few select basis functions as discussed in Chapter III.

For the total fields in region I, we employ the equivalence principle [16] to replace the aperture by an equivalent magnetic surface current source distribution just above a perfectly conducting surface which short-circuits the aperture. Then, convolving this equivalent source distribution with respect to a perfectly conducting half-space Green's function, $j/2\ H_0^{(2)}(k|\bar{\rho}-\bar{\rho}'|)$, we find the fields in region I (y>0) to be

$$u_{s_h}(x,y) = u_{s_h}^{i}(x,y) + u_{s_h}^{r}(x,y)$$

$$\mp \int_{-a}^{a} dx' \left| \begin{matrix} \frac{\partial}{\partial y'} \left[j/2\, H_0^{(2)}(k|\bar{\rho}-\bar{\rho}'|) \right] \cdot u_s(x',y') \\ j/2\, H_0^{(2)}(k|\bar{\rho}-\bar{\rho}'|) \cdot \frac{\partial u_h}{\partial y'}(x',y') \end{matrix} \right| \Bigg|_{y'=0^+} \qquad (2.2)$$

where $u_{s_h}^{i,r}$ are the incident and reflected fields of the equivalent (short-circuited) problem, and where

$$|\bar{\rho}-\bar{\rho}'| = \sqrt{(x-x')^2 + (y-y')^2} \quad . \qquad (2.3)$$

For the fields in region II (cavity region) we employ the equivalence principle to replace the aperture by an equivalent magnetic surface current source distribution just below the short-circuited aperture. Then, integrating the equivalent sources over the Green's function, G_{s_h}, for the short-circuited cavity, we find the fields in region II ($y<0$) to be

$$u_{s_h}(x,y) = \mp \int_{-a}^{a} dx' \left| \begin{matrix} \frac{\partial G_s}{\partial y'}(x,y,;x',y') \cdot u_s(x',y') \\ G_h(x,y;x',y') \cdot \frac{\partial u_h}{\partial y'}(x',y') \end{matrix} \right| \Bigg|_{y'=0^-} \quad . \qquad (2.4)$$

The cavity Green's functions, G_{s_h}, are discussed in the next section.

The equivalent source distributions of Equations (2.2) and (2.4) may be readily interpreted as equivalent magnetic currents by noting that $u_s(x',y')\big|_{y'=0}$ is the z-directed aperture electric field for the TM_z or soft case and that $\frac{\partial u_h}{\partial y'}(x',y')\big|_{y'=0}$ is proportional to the x-directed aperture electric field for the TE_z or hard case.

respectively. The equivalent magnetic surface currents are then obtained from

$$\bar{M}_s^{eq} = \bar{E} \times \hat{n} \tag{2.5}$$

where $\hat{n} = \hat{y}$ for region I and $n = -\hat{y}$ for region II. The equivalent currents for the 2 regions, denoted by $\bar{M}_I$ and $\bar{M}_{II}$, are qualitatively shown in Figures 2.2a and 2.2b for the hard and soft polarizations, respectively. Note that for the hard polarization the current is z-directed, while for the soft polarization it is x-directed.

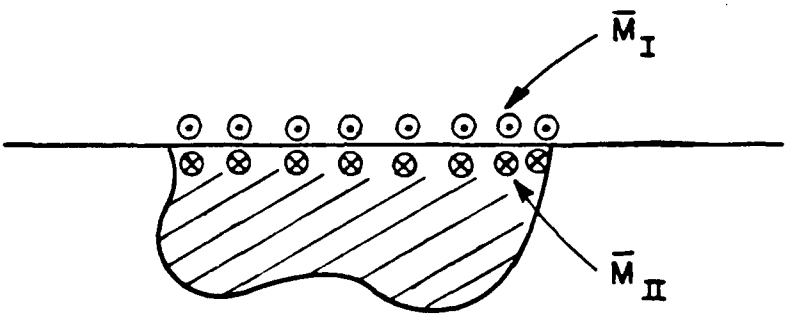

(a) Equivalent magnetic currents for hard polarization.

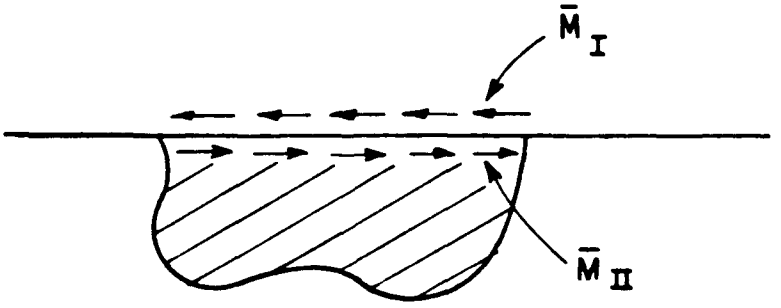

(b) Equivalent magnetic currents for soft polarization.

Figure 2.2. Equivalent magnetic current sources in the aperture region of a cavity recessed in a ground plane.

To arrive at integral equations in which the unknowns are the aperture electric fields, we equate the fields as given by Equations (2.2) and (2.4) in the aperture. Continuity of tangential $\bar{E}$ and $\bar{H}$ fields across the aperture implies the following relations:

$$u_{s,h}(x,y=0^+) = u_{s,h}(x,y=0^-) \tag{2.6a}$$

$$\frac{\partial u_h}{\partial y}(x,y)\Big|_{y=0^+} = \frac{1}{\varepsilon_r}\frac{\partial u_h}{\partial y}(x,y)\Big|_{y=0^-} \tag{2.6b}$$

$$\frac{\partial u_s}{\partial y}(x,y)\Big|_{y=0^+} = \frac{1}{\mu_r}\frac{\partial u_s}{\partial y}(x,y)\Big|_{y=0^-} \tag{2.6c}$$

Since we ultimately will calcuate the fields in region I (y>0), the resulting integral equations are expressed in terms of the aperture fields at $y=0^+$. For the hard polarization we obtain the integral equation

$$\int_{-a}^{a} dx' \left[j/2\, H_0^{(2)}(k|x-x'|) - \varepsilon_r\, G_h(x,x')\right] \frac{\partial u_h(x',y')}{\partial y'}\Big|_{y'=0^+}$$

$$= -2\, u_h^i(x,0) \quad . \tag{2.7}$$

Note that in deriving Equation (2.7) we have used Equations (2.6a) and (2.6b) to enforce the continuity of tangential $\bar{H}$ and tangential $\bar{E}$, across the aperture, respectively.

To derive an integral equation for the soft polarization we take $\frac{\partial}{\partial y}$ of Equations (2.2) and (2.4) and equate the results in the aperture. The continuity relations (2.6a) and (2.6c) are applied to ensure

continuity of tangential $\bar{E}$ and tangential $\bar{H}$, respectively. The resulting integral equation is

$$\int_{-a}^{a} \left[-j/2 \frac{\partial^2}{\partial y \partial y'} H_0^{(2)}(k|\bar{\rho}-\bar{\rho}'|) \Big|_{\substack{y'=0^+ \\ y=0^{++}}} + \frac{1}{\mu_r} \frac{\partial^2}{\partial y \partial y'} G_s(x,y;x',y') \Big|_{\substack{y'=0^- \\ y=0^{--}}} \right] \cdot u_s(x',0)\, dx' = -\frac{\partial}{\partial y} \left[u_s^i(x,y) + u_s^r(x,y) \right] \Big|_{y=0} \qquad (2.8)$$

The derivative $\frac{\partial}{\partial y}$ was necessary for the enforcement of continuity of tangential $\bar{H}$.

Once Equations (2.7) and (2.8) have been solved for their respective equivalent source distributions, the scattered fields in region I may be determined from Equation (2.2) with the short-circuit terms left out. Since we are primarily interested in the far-zone fields, the asymptotic approximation to the Hankel function [17]

$$H_n^{(2)}(k\rho) \sim \sqrt{\frac{2j}{\pi k}}\, j^n \frac{e^{-jk\rho}}{\sqrt{\rho}} \quad ,$$

is used along with the usual approximate form of $|\bar{\rho}-\bar{\rho}'|$ [16]

$$|\bar{\rho}-\bar{\rho}'| \approx \begin{cases} \rho - \hat{\rho}\cdot\bar{\rho}' & \text{in phase} \\ \rho & \text{in amplitude} \end{cases}$$

The scattered fields are then

$$\begin{matrix} u_s \\ h \end{matrix}(\rho,\phi) = \frac{e^{-j\pi/4}}{\sqrt{2\pi k}} \begin{bmatrix} -jk\sin\phi \\ 1 \end{bmatrix} \frac{e^{-jk\rho}}{\sqrt{\rho}} \int_{-a}^{a} e^{jkx'\cos\phi} \begin{bmatrix} u_s(x') \\ \dfrac{\partial u_h(x')}{\partial y'} \end{bmatrix} dx' \qquad (2.9)$$

B. LOADED RECTANGULAR CAVITY RECESSED IN A PERFECTLY CONDUCTING GROUND PLANE

In this section we consider the specific problem to be solved; namely, the scattering of a plane wave from a loaded rectangular cavity recessed in a perfectly-conducting ground plane, as shown in Figure 2.3.

For plane wave incidence, the incident fields may be written in the form

$$u_{sh}^{i}(x,y) = \begin{bmatrix} E_o \\ H_o \end{bmatrix} e^{jkx\cos\phi' + jky\sin\phi'} \quad . \tag{2.10a}$$

Then for the equivalent short-circuited problem, the incident fields are still given by Equation (2.10a), whereas the fields reflected from the short-circuit are given by

$$u_{sh}^{r}(x,y) = \begin{bmatrix} -E_o \\ H_o \end{bmatrix} e^{jkx\cos\phi' - jky\sin\phi'} \tag{2.10b}$$

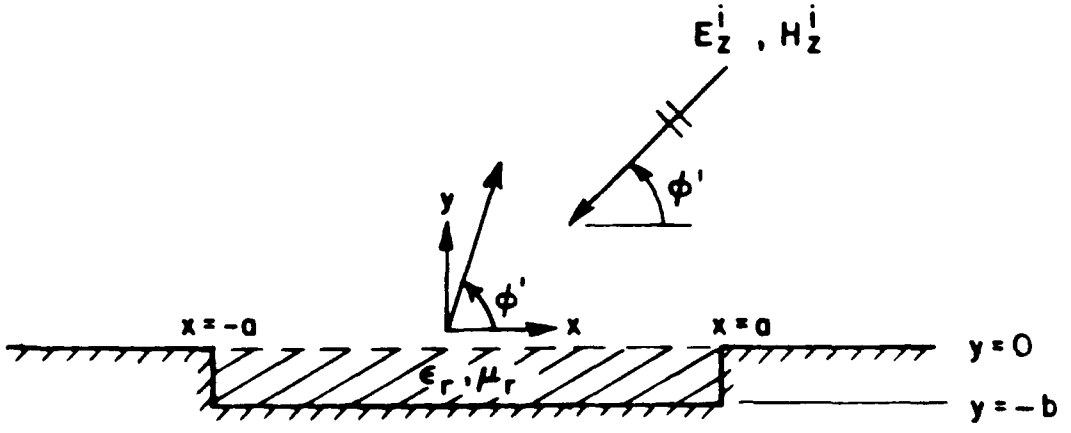

Figure 2.3. Plane wave incidence on a loaded rectangular cavity recessed in a ground plane.

A rigorous derivation of the Green's function for the short-circuited rectangular cavity is given in Appendix B. Here we present the governing relations and the explicit form of $G_{\substack{s \\ h}}$ for the rectangular cavity. The Green's function must satisfy the differential equation

$$\left(\frac{\partial^2}{\partial x^2} + \frac{\partial^2}{\partial y^2} + k^2\, \epsilon_r \mu_r\right) G_{\substack{s \\ h}}(x,y;\, x',y') = -\delta(x-x')\, \delta(y-y') \qquad (2.11a)$$

for all (x,y) and (x',y') within the cavity, and the boundary conditions

$$\left[\begin{array}{c} G_s \\ \dfrac{\partial G_h}{\partial h} \end{array}\right] = 0 \text{ on } C \qquad (2.11b)$$

where C is the contour which defines the enclosed cavity and $\hat{n}$ is the inward normal on C. For the geometry of Figure 2.3 the cavity is defined by y=-b, y=0 and x=-a, x=a.

We solve Equation (2.11a) by separation of variables and an application of the boundary condition (2.11b). Note that the boundary conditions may be applied in two ways: (1) first apply BC's at x=-a, x=a then at y=-b, y=0; or (2) first apply BC's at y=-b, y=0 then at x=-a, x=a.

The first approach may be interpreted as representing the Green's functions, $G_{\substack{s \\ h}}$, interms of the parallel plate waveguide modes propagating in the $\pm\, \hat{y}$ directions and reflecting from the walls at y=-b, y=0. The second approach may be interpreted as representing the $G_{\substack{s \\ h}}$ in terms of the parallel plate waveguide modes propagating in the $\pm\, \hat{x}$ directions and reflecting from the walls at x=-a, x=a. For reasons of convergence

(discussed in Chapter III), the latter approach is used in deriving the cavity Green's functions. The resulting equations are

$$G_s(x,y;x',y') = \frac{-1}{b} \sum_{\ell=1}^{\infty} \frac{\csc 2\gamma a}{\gamma} \left[\cos\gamma(2a-|x-x'|)-\cos\gamma(x+x')\right] \cdot \sin\frac{\ell\pi y}{b} \sin\frac{\ell\pi y'}{b} \tag{2.12a}$$

$$G_h(x,y;x',y') = \frac{-1}{b} \sum_{\ell=0}^{\infty} \frac{\csc 2\gamma a}{\varepsilon_{\ell o}\,\gamma} \left[\cos\gamma(2a-|x-x'|)+\cos\gamma(x+x')\right] \cdot \cos\frac{\ell\pi y}{b} \cos\frac{\ell\pi y'}{b} \tag{2.12b}$$

where

$$\gamma = \begin{cases} \sqrt{k^2\varepsilon_r\mu_r - \left(\frac{\ell\pi}{b}\right)^2}\,, & \ell < \frac{bk}{\pi}\,\mathrm{Re}(\varepsilon_r\mu_r) \\ -j\sqrt{\left(\frac{\ell\pi}{b}\right)^2 - k^2\varepsilon_r\mu_r}\,, & \ell > \frac{bk}{\pi}\,\mathrm{Re}(\varepsilon_r\mu_r) \end{cases} \tag{2.13a,b}$$

and

$$\varepsilon_{\ell o} = \begin{cases} 2\,, & \ell = 0 \\ 1\,, & \ell \neq 0 \end{cases}\,. \tag{2.13c}$$

Note that the other representation of the Green's function is entirely equivalent to Equation (2.12), but is simply not as efficient for the geometry and method of solution presented here.

Before discussing the method of solution to the integral equations, a note should be made concerning the aperture field edge conditions inherent in a geometry such as that of Figure 2.3. These edge conditions are significant since a solution for the aperture fields should at least approximately meet them. It is noted that the edge

behavior can significantly affect the rest of the aperture field distribution; especially for grazing and near-grazing angles of incidence.

Hurd [18] considers the problem of field edge behavior for a conducting wedge in the presence of dielectric wedges. If we are interested in the edge behavior of the aperture electric fields for the geometry of Figure 2.3, then the geometry of Figure 2.4 should be relevant (assuming a non-vanishing cavity). For this geometry Hurd derives the edge conditions

$$E_z = C_1 \rho^t \tag{2.14a}$$

$$E_\rho = C_2 t\rho^{t-1} \tag{2.14b}$$

where

$$t = \frac{2}{\pi} \cos^{-1} \left(\frac{1}{\sqrt{2(\epsilon_r+1)}}\right) \quad . \tag{2.15}$$

Thus, for finite ϵ_r, E_z vanishes at the edge (ρ=0) and E_ρ becomes infinite at the edge.

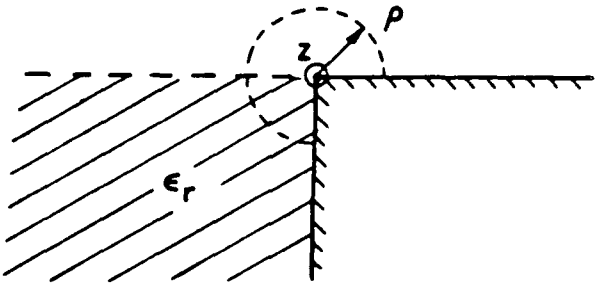

Figure 2.4. Geometry for consideration of edge conditions.

III. SOLUTION OF INTEGRAL EQUATIONS BY THE MOMENT METHOD

A. THE MOMENT METHOD

The moment method [1] is a powerful and frequently used numerical technique for solving integral and integro-differntial equations. It is a method that transforms the integral equation into a matrix equation which is then solved by matrix inversion.

The integral equations (2.7) and (2.8) are of the form

$$\int_a^b G(x,x')\, M(x')\, dx' = F(x) \quad , \qquad a < x,x' < b \quad , \tag{3.1}$$

where G is a known function or operator which constitutes the kernel of the integral equation; F is a known forcing function, and M is the unknown function to be determined. Note that for the problem considered, M is an equivalent magnetic current, F is an incident field (or its derivative), and G is related to the Green's function. The first step in the moment method solution to Equation (3.1) is to expand the unknown function M(x') in a series of basis functions (also called expansion functions) with unknown coefficients. The basis functions may be either subsectional, in which each function spans a subsection of the domain of M(x'), or they may be entire, in which each function spans the the entire domain of M(x'). Some examples of subsectional basis functions are pulses and piecewise-continuous sinusoids. Examples of entire basis functions include Fourier series and other modal

expansions, traveling waves, and functions derived from the geometrical theory of diffractions (GTD) [6] and its uniform version (UTD) [14]. In this work we expand in a series of entire basis functions:

$$M(x') = \sum_{n=1}^{N} D_n M_n(x') \quad , \quad a < x' < b \tag{3.2}$$

where $M_n(x)$ is a basis function and D_n is the corresponding unknown coefficient. Note that as $N \to \infty$, (3.2) can yield a formally exact representation of $M(x')$. For N finite but large the representation is approximate, but nearly-exact results are possible. Substituting (3.2) into (3.1) and assuming that (3.2) is a uniformly convergent expansion,

$$\sum_{n=1}^{N} D_n \int_a^b G(x,x') M_n(x') dx' = F(x) \quad . \tag{3.3}$$

As it stands, Equation (3.3) is a single equation in N unknowns. To convert it to a set of N simultaneous equations in N unknowns, a set of N weighting functions is chosen and applied to Equation (3.3) at N locations in the domain of the weighting function. Thus the second step in the moment method solution is the selection of a set of weighting functions (also called testing functions).

Let $\{w(x), a < x < b\}$ be a set of N weighting functions. Then, we may write the weighted equations as

$$\sum_{n=1}^{N} D_n \int_a^b \int_a^b G(x,x') M_n(x') W_m(x) dx' dx$$

$$= \int_a^b F(x) W_m(x) dx \quad , \quad m = 1, \ldots, N. \tag{3.4}$$

Examples of simple and effective weighting schemes are point-matching and Galerkin's method. In point-matching the weighting functions are simply delta functions,

$$W_m(x) = \delta(x-x_m) \quad , \quad a < x_m < b \quad . \tag{3.5}$$

In Galerkin's method the weighting functions are identical to the basis functions, i.e.,

$$W_m(x) = M_m(x) \quad . \tag{3.6}$$

Equations (3.5) and (3.6) separately constitute the only choices of weighting functions considered in this work.

Equations (3.4) may be expressed in matrix form as

$$[Z_{mn}]\,[D_n] = [V_m] \tag{3.7}$$

where

$$Z_{mn} = \int_a^b \int_a^b G(x,x')\, M_n(x')\, W_m(x)\, dx'\, dx \tag{3.8}$$

$$V_m = \int_a^b F(x)\, W_m(x)\, dx \quad . \tag{3.9}$$

Note that $[Z_{mn}]$ is the so-called impedance matrix and $[V_m]$ is the voltage matrix. Finally, the unknown coefficients are determined from

$$[D_n] = [Z_{mn}]^{-1}\,[V_m] \quad . \tag{3.10}$$

The accuracy of the results depends on the choice of both basis functions and weighting functions. The basis functions should be chosen so that Equation (3.2) can approximate the unknown current M(x') fairly well. The edge conditions and G(x,x') may place restrictions on the useful choice of basis functions. The same restrictions may apply to the weighting functions. Fortunately the moment method is a variational procedure [1] and often yields good results for a wide range of basis and weighting functions.

The moment method is generally considered to be a low-frequency technique limited at present to objects $\lesssim$ 10 wavelengths for two dimensional problems. This limit is a computational one and is due to the large number of unknowns required to accurately model the currents on large, complicated objects. For subsectional basis functions (such as pulses) typically 10-20 unknowns per wavelength are neessary. Appropriate entire basis functions can reduce this by a factor of 2 or more. When the number of unknowns exceeds several hundred, the time and cost required to invert the impedance matrix becomes exhorbitant and the technique is no longer attractive.

In problems where one can identify the dominant physical mechanisms contributing to the unknown current, a hybrid moment method [10],[11], can be a powerful tool. Basis functions are chosen which incorporate the mathematical form of the known physical mechanisms. More traditional basis functions (e.g. pulses) may be used in locations where the physics is not so well understood. The use of these hybrid or traveling wave/GTD basis functions can yield efficient high-frequency

solutions at a cost of increased mathematical complexity. Many excellent examples of this hybrid or traveling wave/GTD approach to the moment method exist in the literature as mentioned earlier.

B. SOLUTION FOR RECTANGULAR CAVITIES OF NARROW TO MODERATE WIDTH AND ARBITRARY DEPTH

In this section we present a solution to the problem depicted in Figure 2.3 which is valid for either loaded or unloaded rectangular cavities of narrow to moderate width and arbitrary depth. This solution requires approximately four unknowns per (free-space) wavelength across the aperture, and is therefore limited to cavities of width ~ 25λ or less.

Entire basis functions are used with a Galerkin weighting scheme. The basis functions are chosen to be the transverse portion of the modes, both propagating and evanescent, of a parllel plate waveguide with plates at x=-a and x=a. This choice of basis functions was also made by Wang [4] in one part of his solution to the scattering by a slot in a thick conducting screen.

The modes supported by a parallel plate waveguide are easily determined from the 2-D scalar wave equation and the boundary conditions at the walls. Expanding the unknowns in the integral Equations (2.7) and (2.8) in terms of the transverse portion of these modes, we obtain for the hard and soft polarizations, respectively,

$$\frac{\partial u_h}{\partial y'}(x') = \sum_{n=0}^{N} D_n \cos\frac{n\pi}{2a}(a-x') \qquad (3.11)$$

$$u_s(x') = \sum_{n=1}^{N} D_n \sin \frac{n\pi}{2a} (a-x') \qquad (3.12)$$

for $-a < x' < a$.

Note that the D_n in (3.11) and (3.12) are in general different.

Applying Galerkin's method we determine the impedance and voltage matrices from Equations (3.8) and (3.9). For the case of hard polarization the results are

$$Z_{mn} = \int_{-a}^{a} \int_{-a}^{a} G(x,x') \cos \frac{n\pi}{2a} (a-x') \cos \frac{m\pi}{2a} (a-x) \, dx'dx \qquad (3.13)$$

$$V_m = -2H_o \int_{-a}^{a} e^{jkx\cos\phi'} \cos \frac{m\pi}{2a} (a-x) \, dx \quad , \qquad (3.14)$$

where $G(x,x')$ equals the quantity in brackets on the LHS of Equation (2.7). Similarly, the results for the soft polarization are

$$Z_{mn} = \int_{-a}^{a} \int_{-a}^{a} G(x,x') \sin \frac{n\pi}{2a} (a-x') \sin \frac{m\pi}{2a} (a-x) \, dx'dx \qquad (3.15)$$

$$V_m = 2jk\sin\phi' \, E_o \int_{-a}^{a} e^{jkx\cos\phi'} \sin \frac{m\pi}{2a} (a-x) \, dx \quad , \qquad (3.16)$$

Where $G(x,x')$ equals the quantity in brackets on the LHS of Equation (2.8). Note that the impedance matrix is symmetric.

The integrals in the expressions for V_m are easily evaluated; however, the double integrals in the expressions for Z_{mn} are considerably more challenging. The mathematical details of this evaluation are given in Appendix C. The double integrals of the Hankel function terms in the total Green's functions are reduced to single integrals by a rotation of coordinates (the so-called Popovich

transformation). The single integrals are evaluated over the initial part by numerical integration and the remaining part is evaluated analytically by using the large-argument form of the Hankel function.

The double integrals of the cavity Green's functions, given by Equations (2.12) and (2.13), can be evaluated in closed form, leaving infinite sums. Specifically for this form of the cavity Green's functions, portions of these infinite sums can be summed into closed form. For the more conventional choice of Green's functions, as given by Equations (B.22) and (B.23), such closed-form terms were not obtained. This fact accounts for the significantly faster convergence for the chosen cavity Green's functions. Only a few evanescent terms are required to achieve numerical convergence of the remaining portion of the sum.

We point out that the current representation given by Equation (3.12) satisfies the edge condition (2.14a) in the sense that (3.12) goes to zero for $|x'|\to a$. Actually each basis function in (3.12) vanishes at the edges of the aperture, a fact which greatly simplifies the evaluation of Z_{mn}. For the hard polarization the current representation given by Equation (3.11) will not go to infinity at the aperture edges as required by (2.14b), assuming a finite value of N. However, (3.11) will approximate the edge condition well enough to yield accurate results even with only four unknowns per wavelength.

Finally, the far-zone scattered fields in region I ($y>0$) are found from Equations (2.9), (3.11) and (3.12) to be

$$u_{\substack{s \\ h}}(\rho,\phi) = \frac{-e^{-j\,\pi/4}}{\sqrt{2\pi k}} \begin{bmatrix} -k\sin\phi \\ 1 \end{bmatrix} \frac{e^{-jk\rho}}{\sqrt{\rho}}$$

$$\cdot \sum_{\substack{n=0 \\ 1}}^{N} \left[\frac{e^{j\,n\pi/2}\sin(k\cos\phi - \frac{n\pi}{2a})a}{k\cos\phi - \frac{n\pi}{2a}} \mp e^{-j\,n\pi/2}\frac{\sin(k\cos\phi + \frac{n\pi}{2a})a}{k\cos\phi + \frac{n\pi}{2a}} \right] \tag{3.17}$$

C. SOLUTION FOR RECTANGULAR CAVITIES OF LARGE WIDTH AND SMALL DEPTH

In this section we present a solution to the problem depicted in Figure 2.3 which is valid for loaded rectangular cavities of large width and small depth. The number of unknowns in this solution is independent of the width of the aperture, but can depend on the depth of the cavity. By small depth it is meant that the dielectric portion of Figure 2.3 will support at most one surface wave mode.

In the previous section, a solution involving a current expansion in parallel plate waveguide modes was presented. This solution will also work for the present case of wide, shallow cavities, but it will require many unknowns (3-4 per wavelength across the aperture). By considering the physics of the wide, shallow cavity we can arrive at a more efficient set of basis functions.

Consider the grounded dielectric slab shown in Figure 3.1. This structure can support surface waves, incident and reflected geometrical optics fields, plus other types of waves which we are not concerned with here. For the case of plane wave incidence the total field in the

region above the slab is simply the incident plus reflected geometrical optics terms (since a plane wave cannot excite surface waves in an infinite dielectric slab):

$$u_{\substack{s \\ h}}(x,y) = \begin{Bmatrix} E_o \\ H_o \end{Bmatrix} \cdot \left[e^{jk(y+b)\sin\phi'} + \Gamma_{\substack{s \\ h}} e^{-jk(y+b)\sin\phi'} \right] \cdot e^{jkx\cos\phi'} \tag{3.18}$$

where the reflection coefficient is [19]

$$\Gamma_h = \frac{j\,\varepsilon_r\,\mu_r\,\sin\phi' + h \cdot \tan(kbh)}{j\,\varepsilon_r\,\mu_r\,\sin\phi' - h \cdot \tan(kbh)} \tag{3.19a}$$

$$\Gamma_s = \frac{j\,\sin\phi' - h \cdot \cot(kbh)}{j\,\sin\phi' - h \cdot \cot(kbh)} \tag{3.19b}$$

and

$$h = \sqrt{\varepsilon_r\,\mu_r - \sin^2\phi'} \tag{3.20}$$

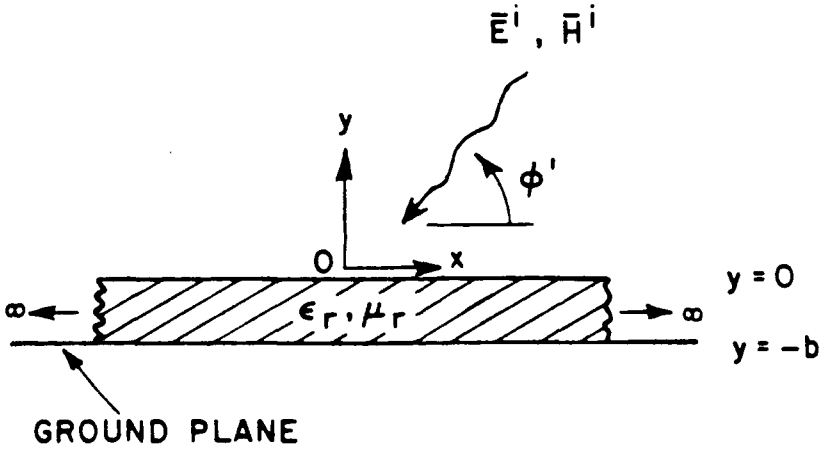

Figure 3.1. Scattering from an infinite dielectric slab on a ground plane.

Note that the reflection coefficient has a magnitude of unity, as we would expect for an incident plane wave.

If we truncate the slab of Figure 3.1, then the diffration of an incident plane wave at the ends of the slab will excite surface waves. The z-components of hard and soft normalized surface waves are [16]

$$u_h = \begin{cases} e^{-\alpha y - j\beta x} & , \quad y > 0 \qquad (3.21a) \\ \dfrac{\cos\alpha_1(y+b)}{\cos\alpha_1 b} \cdot e^{-j\beta x} & , \quad 0 > y > -b \qquad (3.21b) \end{cases}$$

$$u_s = \begin{cases} e^{-\alpha y - j\beta x} & , \quad y > 0 \qquad (3.22a) \\ \dfrac{\sin\alpha_1(y+b)}{\sin\alpha_1 b} \cdot e^{-j\beta x} & , \quad 0 > y > -b \quad , \qquad (3.22b) \end{cases}$$

where 'hard' and 'soft' are as defined by Equation (2.1). The surface wave propagation constant, β, is determined from

$$\alpha_1 \tan \alpha_1 b = \varepsilon_r \alpha \qquad (3.23a)$$

$$-\alpha_1 \cot \alpha_1 b = \mu_r \alpha \qquad (3.23b)$$

for the hard and soft polarizations, respectively, where

$$\alpha^2 = \beta^2 - k^2 \qquad (3.24a)$$

$$\alpha_1^2 = k^2 \varepsilon_r \mu_r - \beta^2 \quad . \qquad (3.24b)$$

Substituting Equations (3.24) into (3.23) yields a transcendental equation in β, which is then solved by the Newton-Raphson method. From Equations (3.23a,b) it may be shown that the first surface wave mode for the hard polarization has no cutoff frequency. This is not true for the

soft polarization. Thus even a very thin grounded dielectric slab will support a surface wave only for a hard-polarized incident field.

We now return to the geometry of Figure 2.3 and consider a suitable choice of basis functions. From the above discussion it seems reasonable to assume that a geometrical optics type of field (also called a forced wave inside the dielectric), such as Equation (3.18), will make a significant contribution to the aperture field. In addition, if we assume the dominant surface wave mode is present, then terms such as (3.21) and (3.22) are also important. Thus far, our expansion for the aperture electric fields is

$$\begin{vmatrix} \overline{\frac{\partial u_h}{\partial y}\ (x)} \\ \overline{u_s\ \ (x)} \end{vmatrix} = D_1\, e^{jkx\cos\phi'} + D_2\, e^{-j\beta x} + D_3\, e^{j\beta x} \quad ;\ |x|<a \qquad (3.25)$$

where β depends on polarization. The coefficients D_2 and D_3 include the multiple reflections of the surface waves from the end walls at x=-a and x=a. Richmond [12] employed a very similar expansion in his moment method solution to scattering by a thin dielectric strip (E_z polarization only).

For this problem considered here the current representation (3.25) does not properly account for the aperture physics near the end walls. The transition region exists between the edges of the aperture and the region where the surface waves become established. This transition region typically extends about one wavelength into the aperture from the edges, except for near grazing angles of incidence where it could

possibly extend over the entire aperture region if the aperture is only moderately wide.

To account for the physics of the transition regions additional basis functions were chosen which were entire but of importance only near the edges. To keep the mathematical complexity to a minimum, a set of exponential functions which decay away from the edges were chosen. Thus the current expansion now becomes

$$\begin{bmatrix} \frac{\partial u_h}{\partial y}(x) \\ u_s(x) \end{bmatrix} = D_1 e^{jkx\cos\phi'} + D_2 e^{-j\beta(a-x)} + D_3 e^{-j\beta(a+x)} + D_4 e^{-jq_1(a-x)} + D_5 e^{-jq_1(a+x)} + D_6 e^{-jq_2(a-x)} + D_7 e^{-jq_2(a+x)} + \ldots \qquad (3.26)$$

where the q_i are empirically determined complex numbers with a negative imaginary component. A discussion of suitable values for the q_i is given in the next chapter; typically there are several transition terms. Note that the surface waves and the transition terms in Equation (3.26) are written in a form that indicates that these terms emanate from the edges of the aperture, whereas the forced wave term is not written in such a form.

Recall that $u_s(x)$ must satisfy the edge condition (2.14a). Thus, for the soft polarization, Equation (3.26) must be set equal to zero at x=-a and x=a. Upon doing this we may then solve for two of the N unknown coefficients in terms of the remaining coefficients, thus

reducing the number of unknowns from N to N-2. The resulting form for a given basis function for the soft polarization becomes

$$M_n(x) = a_n\, e^{-j\theta(a-x)} + e^{j(h_n a + f_n x)} + b_n\, e^{-j\theta(a+x)} \quad , \tag{3.27}$$

where h_n and f_n are the appropriate values of $k\cos\varphi$, β, and q_i shown in Equation (3.26), and θ is an empirically determined complex number with a negative imaginary component (like the q_i), and where

$$a_n = -2j\, e^{j(h_n-\theta)\, a}\, \frac{\sin(f_n+\theta)a}{1-e^{-4j\theta a}} \tag{3.28a}$$

$$b_n = -2j\, e^{j(h_n-\theta)\, a} \cdot \frac{\sin(f_n-\theta)a}{1-e^{-4j\theta a}} \quad . \tag{3.28b}$$

A value of θ is chosen so that the basis function given by Equation (3.27) goes to zero rapidly near the edges of the aperture; a discussion of actual numerical values is deferred to the next chapter. The corresponding form of a given basis function for the hard polarization is

$$M_n(x) = e^{j(h_n a + f_n x)} \quad . \tag{3.29}$$

Applying Galerkin's method we determine the impedance and voltage matrices from Equations (3.8) and (3.9). For the hard polarization the results are

$$Z_{mn} = \int_{-a}^{a} \int_{-a}^{a} G(x,x')\, e^{j(h_n a + f_n x')}\, e^{j(h_m a + f_m x)}\, dx'dx \tag{3.30}$$

$$V_m = -2H_o \int_{-a}^{a} e^{jkx\cos\phi'} \, e^{j(h_m a + f_m x)} \, dx \qquad (3.31)$$

where G(x,x') equals the quantity in brackets on the LHS of Equation (2.7). Similarly the results for the soft polarization are

$$Z_{mn} = \int_{-a}^{a} \int_{-a}^{a} G(x,x') \left[a_n \, e^{-j0(a-x')} + e^{j(h_n a + f_n x')} + b_n \, e^{-j0(a+x')} \right] \cdot \left[a_m \, e^{-j0(a-x)} + e^{j(h_m a + f_n x)} + b_m \, e^{-j(a+x)} \right] dx'dx \qquad (3.32)$$

$$V_m = -2jk \sin\phi' \, E_o \int_{-a}^{a} e^{jkx\cos\phi'} \cdot \left[a_m \, e^{-j0(a-x)} + e^{j(h_m a + f_m x)} + b_m \, e^{-j0(a+x)} \right] dx \qquad (3.33)$$

where G(x,x') equals the quantity in brackets on the LHS of Equation (2.8). Note that the impedance matrix is symmetric.

Again the expressions for V_m are easily evaluated. Comparing the above expressions for the impedance matrix elements with those of the waveguide mode current expansion, given by Equations (3.13) and (3.15), we see that in both cases the basis and weighting functions may be expressed as exponentials. Thus, the evaluation of Equations (3.30) and (3.32) is not fundamentally different from that of Equations (3.13) and (3.15).

Finally the far-zone scattered fields in region I (y>0) are found from Equations (2.9), (3.27) and (3.29) to be

$$u_s(\rho,\phi) = \frac{-e^{-j\,\pi/4}}{\sqrt{2\pi k}}\,(-k\sin\phi)\,\frac{e^{-jk\rho}}{\sqrt{\rho}} \cdot 2 \cdot \sum_{n=1}^{N-2} \cdot \left[a_n\, e^{-j0a} \cdot \right.$$

$$\frac{\sin(k\cos\phi+0)a}{k\cos\phi+0} + e^{jh_n a} \cdot \frac{\sin(k\cos\phi+f_n)a}{k\cos\phi+f_n}$$

$$\left. + b_n\, e^{-j0a} \cdot \frac{\sin(k\cos\phi-0)a}{k\cos\phi-0} \right] \qquad (3.34)$$

for the soft polarization, and

$$u_h(\rho,\phi) = \frac{-e^{-j\,\pi/4}}{\sqrt{2\pi k}} \cdot \frac{e^{-jk\rho}}{\sqrt{\rho}} \cdot 2 \sum_{n=1}^{N-2} \cdot \left[e^{-jh_n a} \cdot \frac{\sin(k\cos\phi+f_n)a}{k\cos\phi+f_n} \right] \qquad (3.35)$$

for the hard polarization.

IV. NUMERICAL RESULTS AND DISCUSSION

A. CAVITIES OF ARBITRARY DEPTH AND NARROW TO MODERATE WIDTH RECESSED IN A GROUND PLANE

In this section we consider the EM scattering from loaded or unloaded cavities of narrow to moderate width and recessed an arbitrary distance in a ground plane. By "narrow to moderate width" it is meant that the aperture width is $\lesssim 10\ \lambda$, where λ is the free-space wavelength.

Before discussing the numerical results in this section, it is important to introduce an explanation of the titles, labels and variable names that accompany each of the computer plots pertaining to the numerical calculations presented below.

TITLES OF PLOTS

PMH = pulses/point matching solution for hard polarization

NOTCHH, NOTCHS = hybrid basis solution for hard, soft polarization

(ignore the .TEST appearing in some titles)

COORDINATE LABELS

BACKSCATTER = monostatic backscattered field (E_z or H_z) magnitude multiplied by the factor $\sqrt{\pi k}$, where k is the free-space wavenumber.

MAGNITUDE, PHASE = equivalent current magnitude and phase

PATTERN MAGNITUDE = bistatic scattered field (E_z or H_z)

VARIABLES COMMON TO ALL SOLUTIONS

WIDTH = aperture width, λ (free-space)

DEPTH = cavity depth, λ

ERR = Re (ε_r) in the dielectric loading of the cavity

ERI = Im (ε_r) in the dielectric loading of the cavity

URR = Re (μ_r) in the dielectric loading of the cavity

URI = Im (μ_r) in the dielectric loading of the cavity

PHP = ϕ', $0° < \phi' < 90°$ ($\phi'=90°$ => normal incidence.)

VARIABLES SPECIFIC TO A SOLUTION

PMH = MM solution using pulse expansion and point matching in the aperture only for the hard case

NMODE = Number of modes in the cavity Green's function (modes propagating in $\pm \hat{y}$ direction)

PW = Pulse width, λ

N1,N2 = Number of pulses counting from x=-a, x=+a.

NOTCHH,NOTCHS = Hard and soft case MM solutions using modal expansion in waveguide aperture respectively

NZ1,NZ = Number of unknown modal basis functions for hard, soft polarization

NMODE = Number of terms in reduced form of cavity Green's function (modes propagating in $\pm \hat{x}$)

DX = 2 * integration step of numerical portion of integration, λ

EWAVH3,EWAVS = Hard and soft case MM solution using a hybrid traveling wave expansion in the aperture, respectively.

NMODE = Same as for NOTCHH,NOTCHS

DX = Same as for NOTCHH,NOTCHS

NFW = Number of forced wave basis functions

NSW = 1/2 number of surface wave basis functions

NEW = 1/2 number of transition term basis functions

We first consider results for the hard polarization. Figure 4.1 compares a pulse/point-matching solution for the monostatic scattered magnetic field (H_z) from a loaded recessed cavity of width=1λ, depth=0.1λ to the Galerkin solution employing entire waveguide mode basis functions (Chapter III, Section B). The pulses/point-matching solution employs 20 pulses of width=0.05λ and 10 modes in the cavity Green's function (using the form given by Equation (B.22b); the CPU time on a PRIME computer was 49 seconds. The modal basis solution employs 5 waveguide modes, no modes in the expression for Z_L of (C.12) (the closed-form portion of Z_L proved to be sufficient), and a numerical integration step of 0.05λ; the CPU time was 15 seconds. Note that both solutions were verified to have converged. Similar results are given in Figure 4.2 for a depth=10.1λ. Again, there is good agreement between

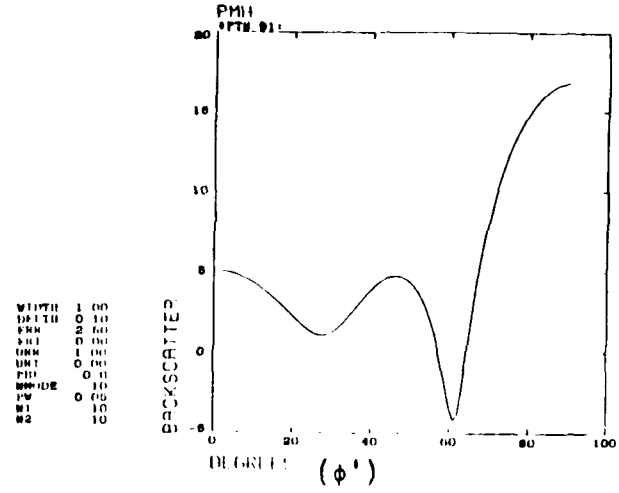

(a)

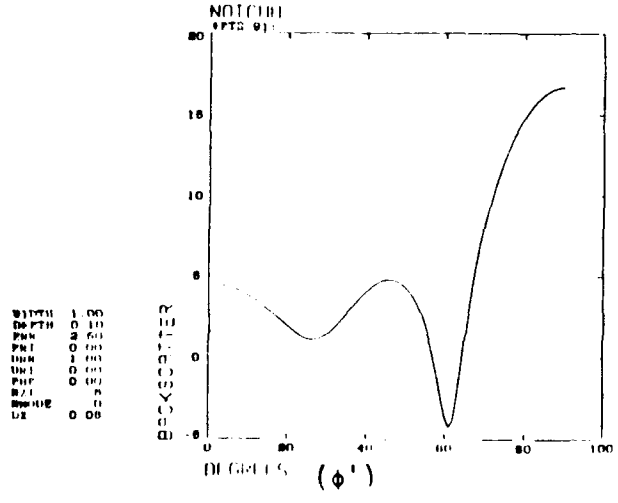

(b)

Figure 4.1. Backscattering by a notch type cavity in a ground plane.

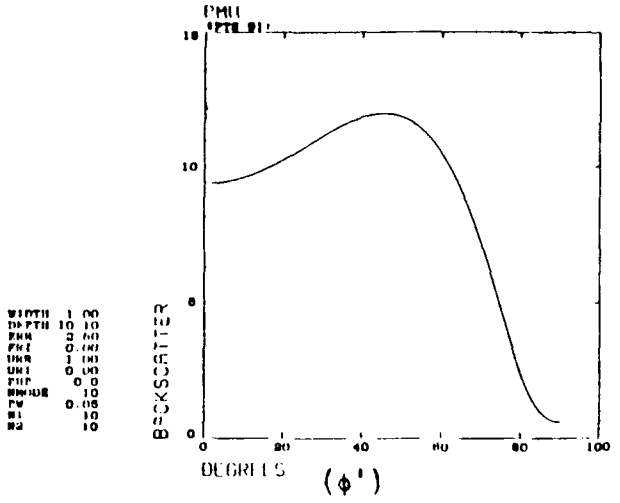

(a)

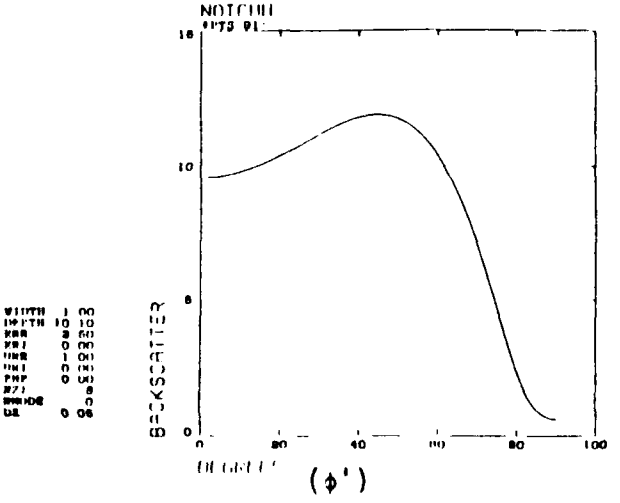

(b)

Figure 4.2. Backscattering by a deep notch cavity in a ground plane.

the solutions. Note that even for the deep cavity, no modes were required for the computation of Z_L.

Now consider the soft polarization. Figures 4.3 and 4.4 show the monostatic scattered electric field (E_z) computed from the modal basis method for cavities of depth = 0.1λ and 10.1λ, respectively. This solution employs 4 waveguide modes, no modes in the expression for Z_L (again, the closed-form portion of Z_L was sufficient), and an integration step of $.05\lambda$. Bistatic scattered field equivalent currents and far-field patterns computed with the modal basis solution were compared with a moment method solution [4] employing piecewise continuous sinusoids and Galerkin's method. Good agreement was observed for the two solutions for normal incidence. There appears to be some question as to the use of the computer codes in [4] for grazing angles; hence, this comparison has not been made at this time.

B. LOADED SHALLOW CAVITIES OF LARGE WIDTH RECESSED IN A GROUND PLANE

In this section we consider scattering from loaded shallow cavities of large width ($\geq 5\ \lambda$) recessed in a ground plane. By "shallow" it is meant that at most one surface wave is supported in the dielectric. This condition places constraints on the depth of the cavity and the electrical properties of the dielectric medium according to Equations (3.23) and (3.24). Table 4.1 shows surface wave propragation constants as a function of dielectric thickness (i.e., cavity depth) for a dielectric with $\varepsilon_r 2.5$, $\mu_r = 1.0$. A dash (-) indicates that a surface wave is not supported.

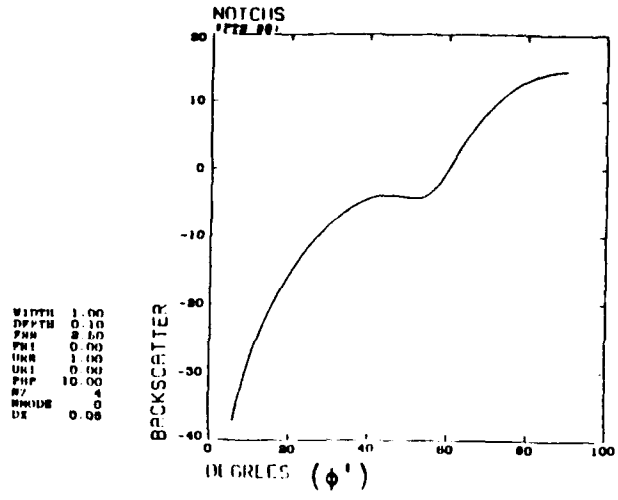

Figure 4.3. Backscattering by a notch type cavity in a ground plane.

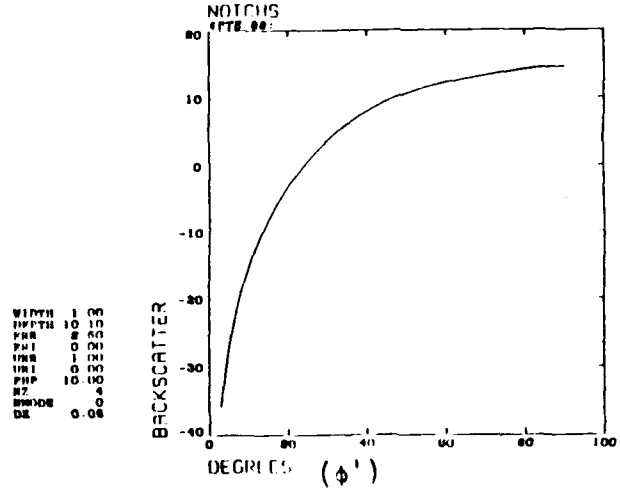

Figure 4.4. Backscattering by a deep notch cavity in a ground plane.

TABLE 4.1

HARD AND SOFT SURFACE WAVE PROPAGATION CONSTANTS FOR A GROUNDED DIELECTRIC WITH ε_r=2.5, μ_r=1.0 AS A FUNCTION OF DIELECTRIC THICKNESS

b	β_h	β_s
.05 λ	6.399 λ^{-1}	--
.10	6.789	--
.15	7.442	--
.20	8.105	6.288
.25	8.599	6.630

Figure 4.5 compares a pulses/point-matching solution to the modal basis solution for the monostatic scattered magnetic field from a loaded recessed cavity of width=5λ, depth=.05λ, ε_r=2.5. The pulses/point-matching solution employs 50 pulses of width=.10λ and 40 modes in the cavity Green's function; the CPU time was 9 minutes, 47 seconds. The modal basis solution employs 21 waveguide modes, only the closed-form term in Z_L, and an integration step of .05λ; the CPU time was 1 minute, 10 seconds. The modal basis solution was observed to converge. Due to lack of disk space we were unable to verify the convergence of the point matching solution.

Also shown in Figure 4.5, at ten degree intervals, is the solution obtained using the basis functions discussed in Section C of Chapter III. This solution employs a forced wave, two surface waves, and 8 transition terms for a total of 11 basis functions, and is valid for any cavity width larger than a few wavelengths. The surface wave propagation constant for this geometry is given in Table 4.1. The transition term "propagation" constants were chosen to be of the form

$$q_i = k - js_i \quad , \tag{4.1}$$

where the q_i are defined in Equation (3.26), k is the free-space wavenumber, and the s_i are empirically determined attenuation constants. It was found from numerical experimentation that allowing the s_i to take on the four integer values

$$s_i = 5,6,7,8 \quad , \tag{4.2}$$

resulted in accurate monostatic scattered fields for shallow cavities. Actually, the nonostatic scattered field is somewhat insensitive to the specific q_i chosen, as long as the corresponding basis functions are insignificant a wavelength or so from the aperture edge. The CPU time for the points shown in Figure 4.5 was 1 minute, 16 seconds, which is similar to the CPU required for the modal basis solution. Even though fewer unknowns are required in the hybrid basis solution (11 versus 21 in the modal basis solution), one of the basis functions, the forced wave, is a function of the angle of incidence, as can be seen from Equation (3.26). Thus, a row of the impedance matrix must be recomputed and the resulting matrix inverted for each new angle of incidence. In the modal basis solution the impedance matrix is computed and inverted

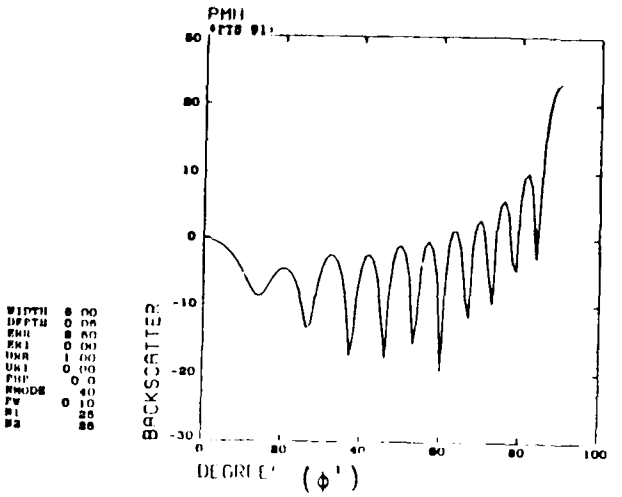

(a)

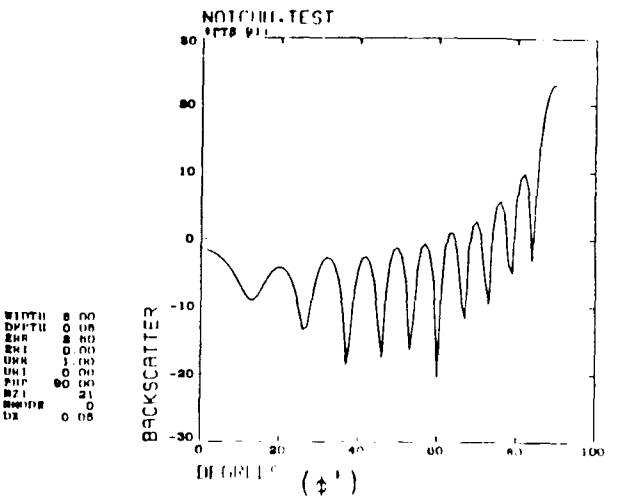

(b)

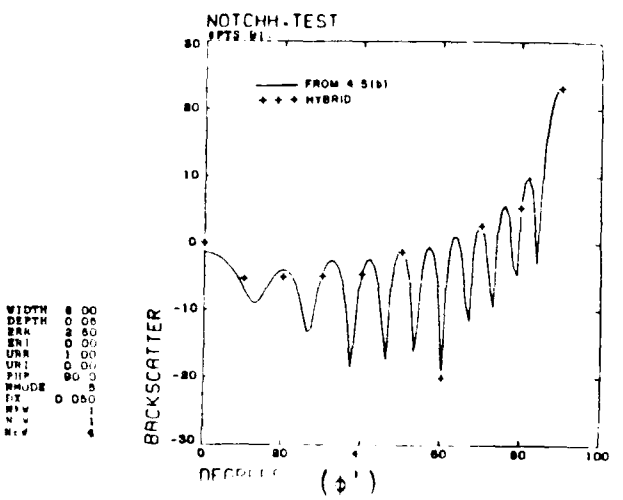

(c)

Figure 4.5. Backscattering by a wide and shallow cavity.

only once. The advantage of the hybrid basis solution is, of course, that only 11 unknowns are required regardless of cavity width.

Figures 4.6 and 4.7 compare the hybrid and modal basis solutions for the equivalent magnetic aperture current and bistatic scattered field pattern for a plane wave normally incident on the geometry of Figure 4.5, except that the cavity depth=0.10λ. The required CPU for the modal basis solution was 54 seconds; versus 28 seconds for the hybrid basis. Figures 4.8 and 4.9 make the same comparison for grazing incidence ($\phi'=0°$). Note that excellent agreement between the two solutions even for grazing incidence.

Figures 4.10 to 4.13 compare the monostatic scattered field obtained from the hybrid basis solution at ten degree intervals to the modal basis solution for cavity depths of .10λ, .15λ, .20λ, and .25 λ. Good agreement is obtained everywhere except for the grazing incidence region for a depth of .25λ, the largest depth which was tried. Such variations might yield good results for a particular geometry, but would not always apply to other geometries. Thus, a consistent method for choosing exponential-type transition terms was not found for the deeper cavities, i.e., for depth=.20λ and .25λ. In short, an accurate and very efficient hybrid solution for the hard polarization was found for cavities with depths less than .15λ and of arbitrary width.

Consider now the soft polarization results of plane wave scattering from the same geometry considered in the above hard polarization analysis. From Table 4.1 one sees that surface waves do not exist in

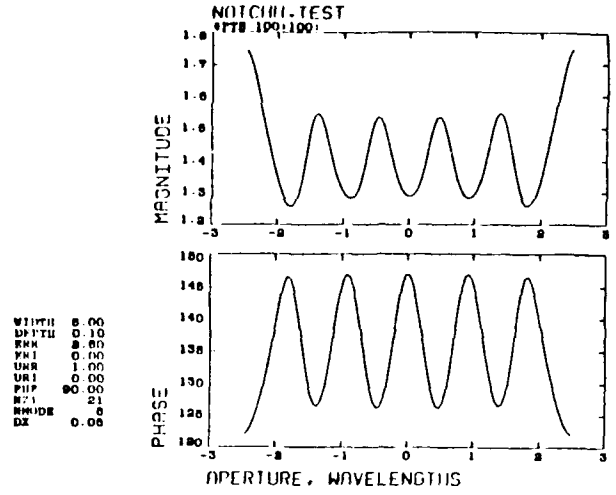

(a)

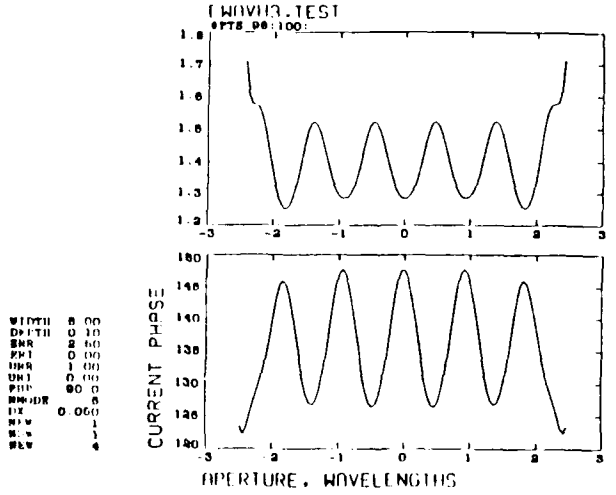

(b)

Figure 4.6. Current distribution on the aperture of a wide and shallow cavity for normal incidence.

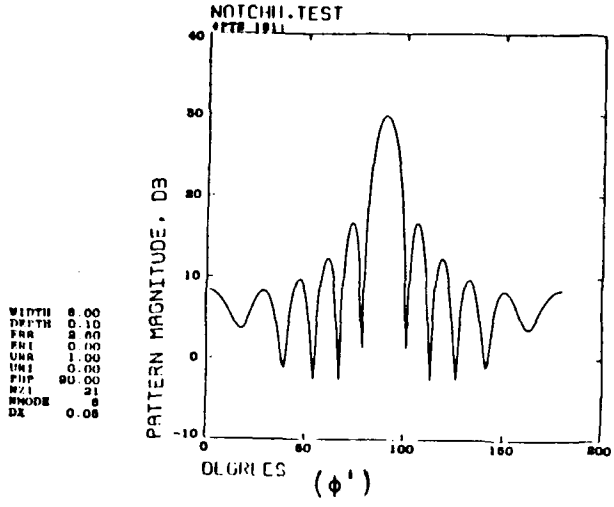

(a)

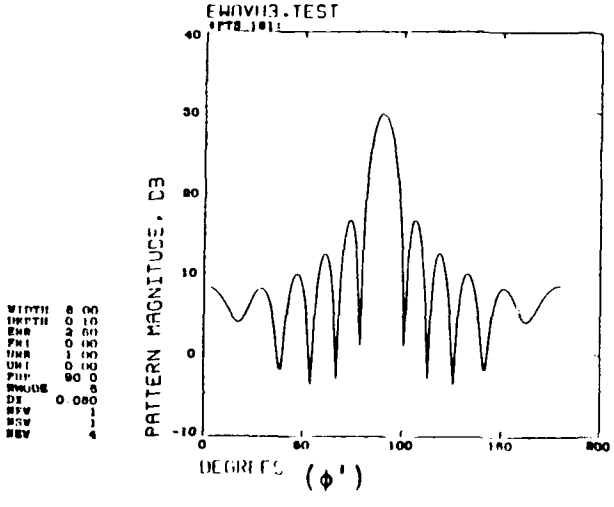

(b)

Figure 4.7. Bistatic scattering for normal incidence on a wide and shallow cavity.

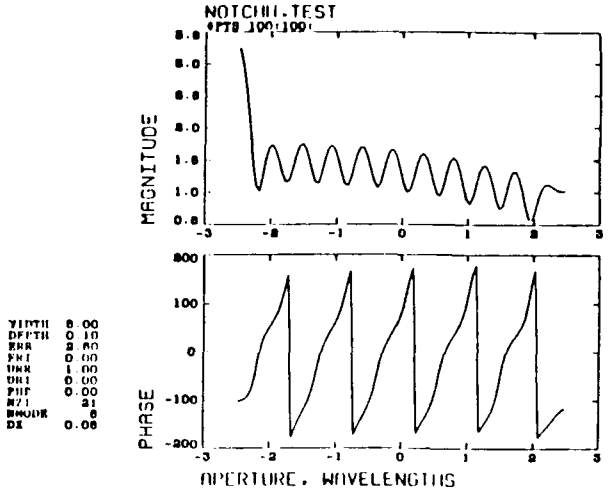

(a)

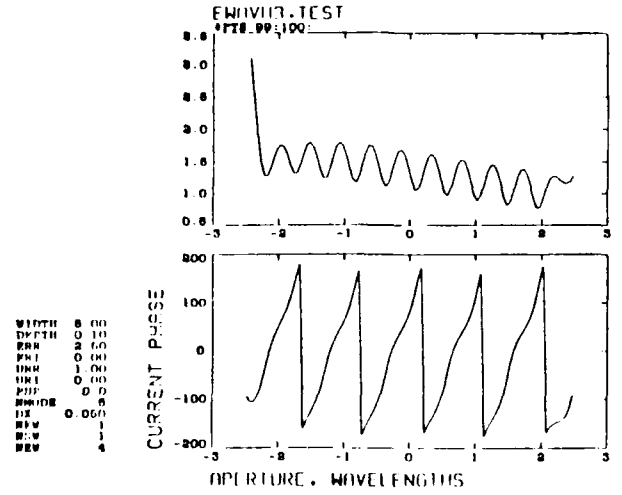

(b)

Figure 4.8. Current distribution in the aperture of a wide and shallow cavity for grazing incidence.

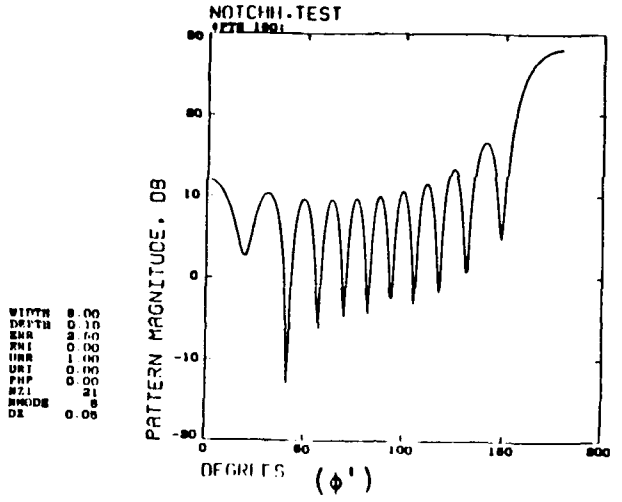

(a)

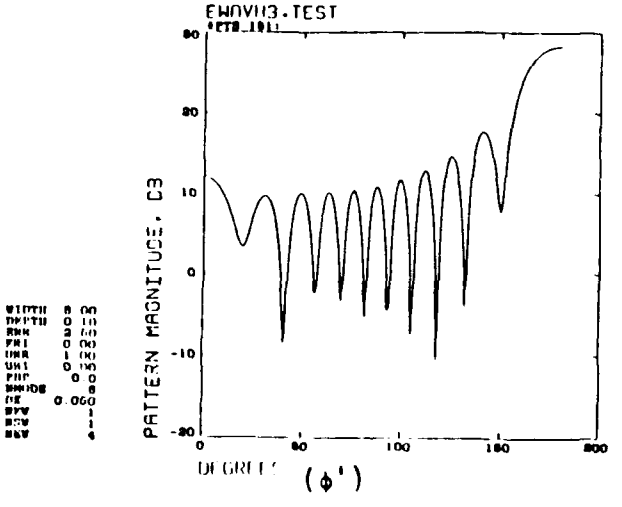

(b)

Figure 4.9. Bistatic scattering by a wide and shallow cavity for grazing incidence.

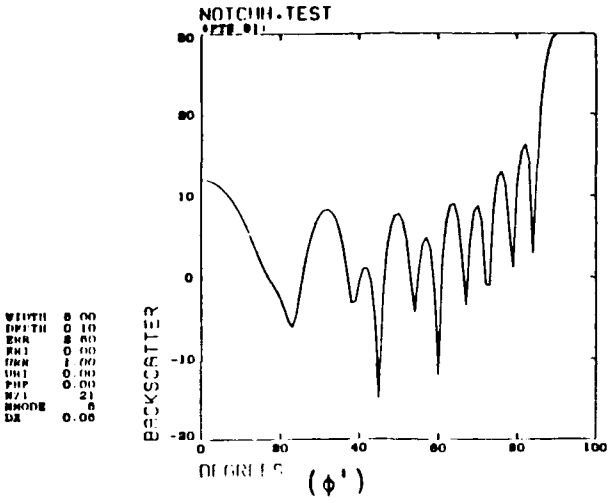

(a)

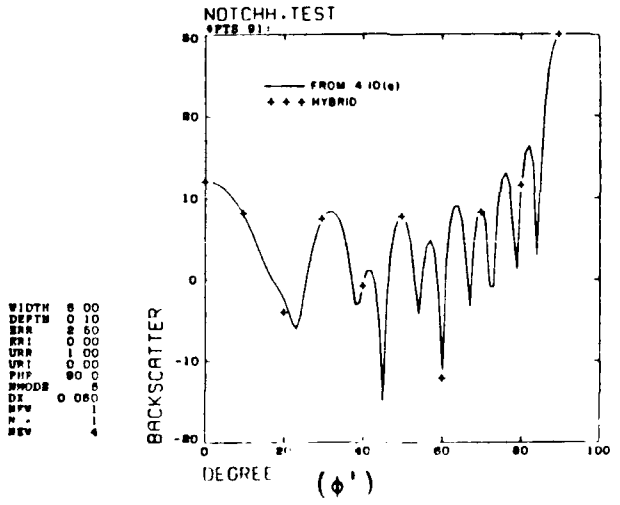

(b)

Figure 4.10. Backscattering by a wide and shallow cavity.

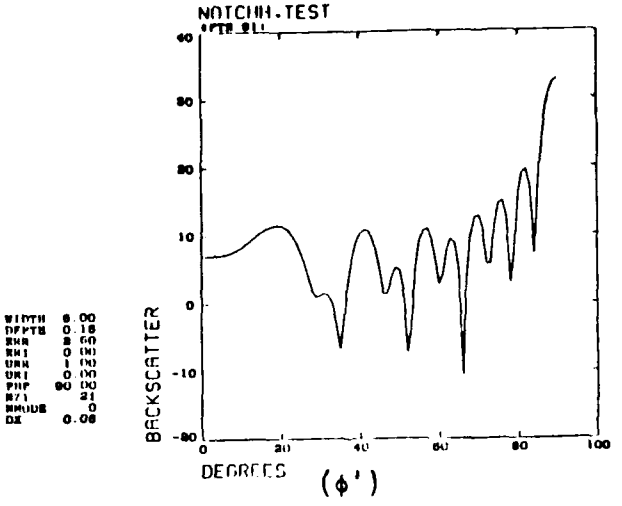

(a)

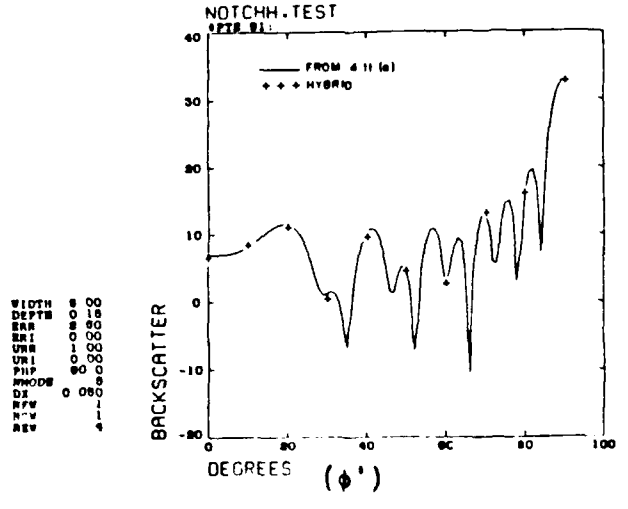

(b)

Figure 4.11. Backscattering by a wide and shallow cavity.

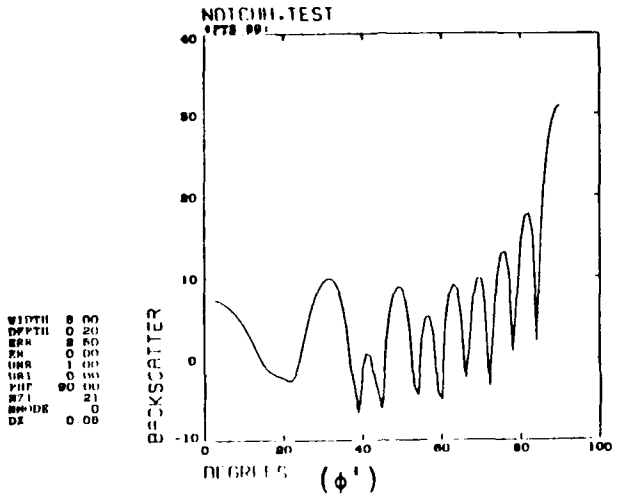

(a)

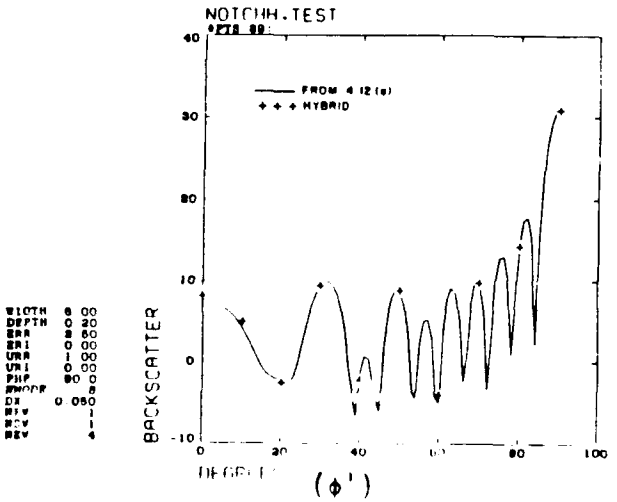

(b)

Figure 4.12. Backscattering from a wide and shallow cavity.

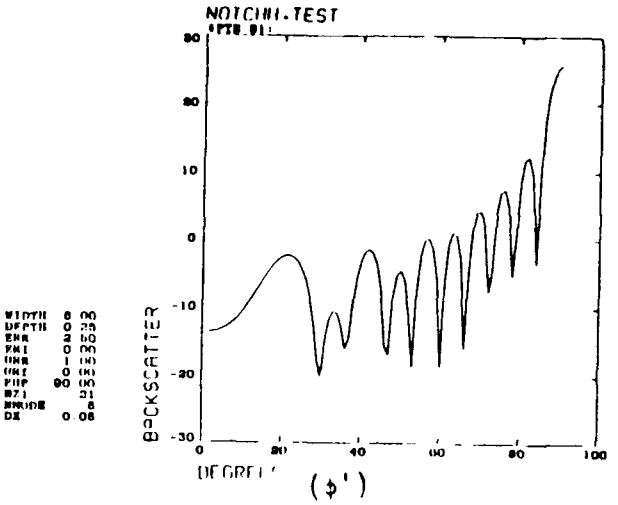

(a)

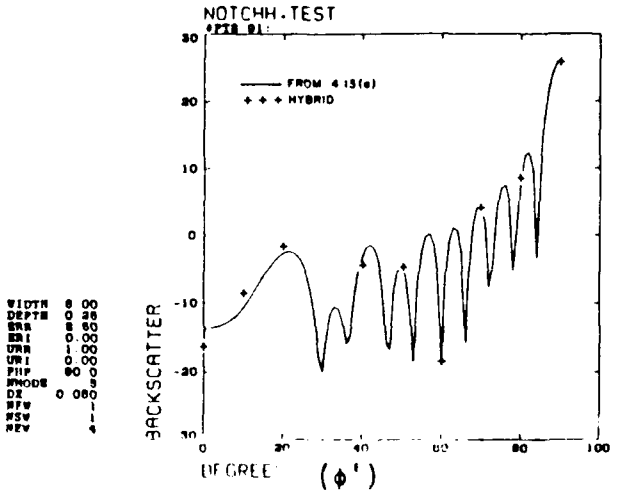

(b)

Figure 4.13. Backscattering from a wide and shallow cavity.

the thin dielectrics for the material properties ε_r=2.5, μ_r=1.0. However, a transition surface wave type of field does exist under cutoff conditions. From plots of the equivalent currents in the aperture it is readily apparent that this field has the propagation constant of free space and becomes more significant as cutoff of the dominant surface wave is approached. For a depth of .15λ and .10λ it is less obvious. For this reason a "surface wave" with propagation constant=k will be employed in the hybrid basis solution for the recessed cavity of depth=.15λ, even though the dominant surface wave is actually cutoff.

Figure 4.14 compares the hybrid basis solution to the modal basis solution for the monostatic scattered electric field from a loaded recessed cavity of width=5λ and depth=.05λ. The modal basis solution employs 20 modes; the CPU time was 1 minute 7 seconds. Because of the fundamental similarity between the modal basis solutions for the hard and soft polarizations, the CPU times are nearly identical for a given number of unknowns. The hybrid basis solution employs only a forced wave. However, recall that additional exponential terms are employed so that each basis function will meet the edge condition. Thus, for a basis function of the form given by Equation (3.27), a value of 0 must be chosen so that the basis function will go to zero in an appropriate manner as $|x| \to a$. A suitable form for 0 is

$$0 = k - js \quad . \tag{4.3}$$

where k is the free-space wavenumber, and s is determined empirically. The value of s used in Figure 4.14 and the following figures is

$$s = 6 \tag{4.4}$$

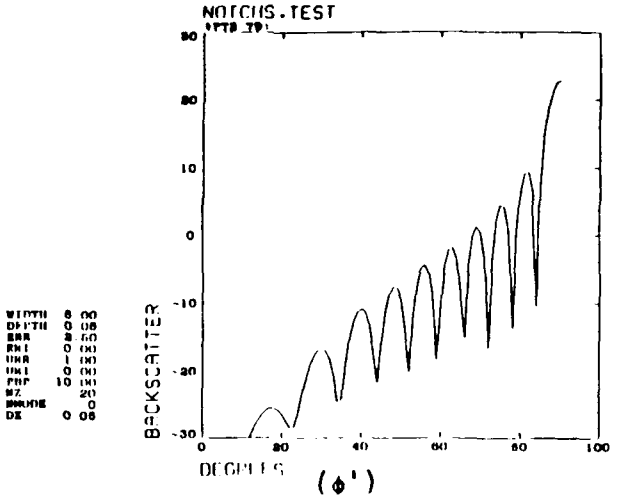

(a)

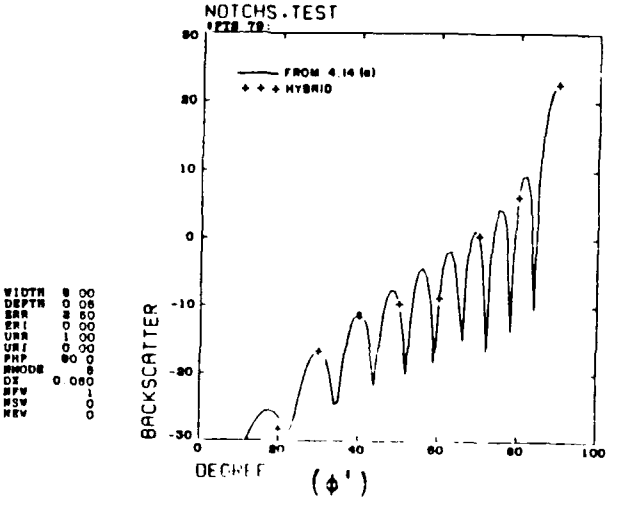

(b)

Figure 4.14. Backscattering by a wide and shallow cavity.

However, numerical experimentation has shown that the hybrid basis solution is quite insensitive to specific value of 0. Any choice of 0 which takes the basis function to zero within a fraction of wavelength of the edge is suitable. Note that the exponential transition terms used in the hybrid basis solution for the hard polarization were not found to be useful for the soft polarization, except as a means of enforcing the edge condition.

Because there is only one unknown in the hybrid basis solution shown in Figure 4.14, the CPU time is only 20 seconds.

The agreement between the hybrid basis and modal basis solutions in Figure 4.14 is very good except near grazing incidence. This disparity is more clearly illustrated in the next set of figures. Figures 4.15 to 4.18 compare the equivalent aperture currents and bistatic scattered field patterns of the two solutions for angles of incidence $\phi'=90°$ and $\phi'=10°$ and a cavity of depth=.10λ. Again, only the forced wave is employed in the hybrid basis solution, and 20 modes are employed in the modal basis solution; the CPU times are 8 seconds and 50 seconds respectively. The agreement for $\phi'=90°$ is very good, although from Figure 4.15 one can see that a weak field is present in addition to the forced wave portion of the total field. This additional field is more significant for $\phi'=10°$, as can be readily seen in Figure 4.17. The corresponding bistatic scattered field patterns, shown in Figure 4.18, display good agreement except for the region of grazing incidence, $\phi'<30°$. Attempts to improve the solution in this region by the addition of a surface wave with propagation constant k and/or the inclusion of exponential transition terms were unsuccessful.

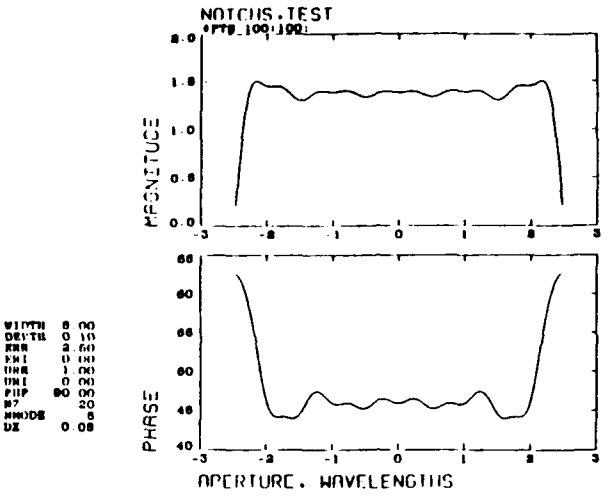

(a)

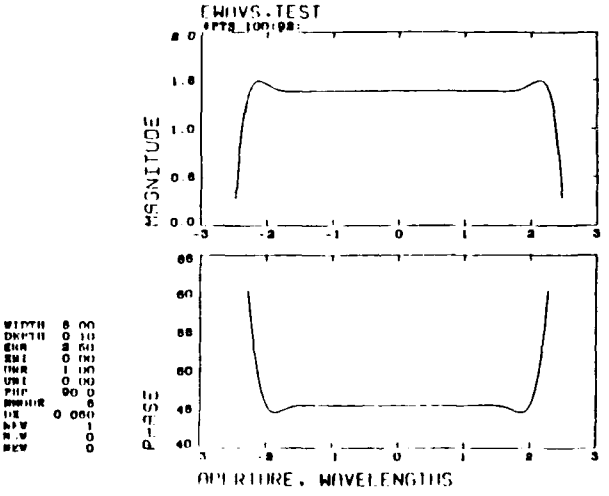

(b)

Figure 4.15. Current distribution in the aperture of a wide and shallow cavity for normal incidence.

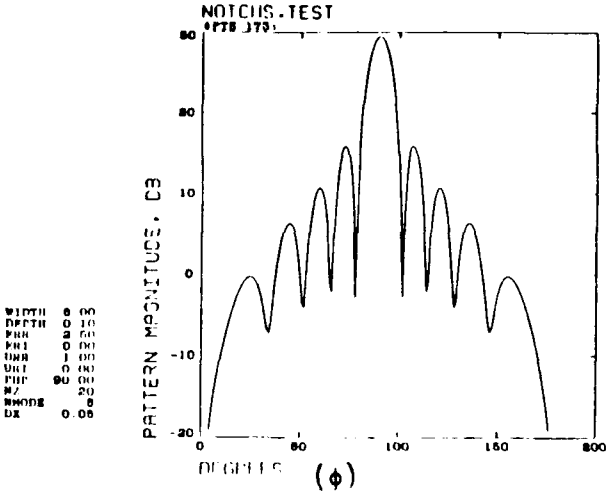

(a)

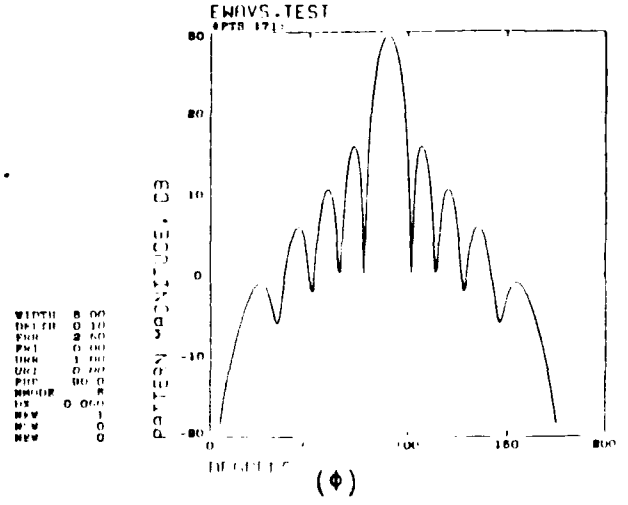

(b)

Figure 4.16. Bistatic scattering by a wide and shallow cavity for normal incidence.

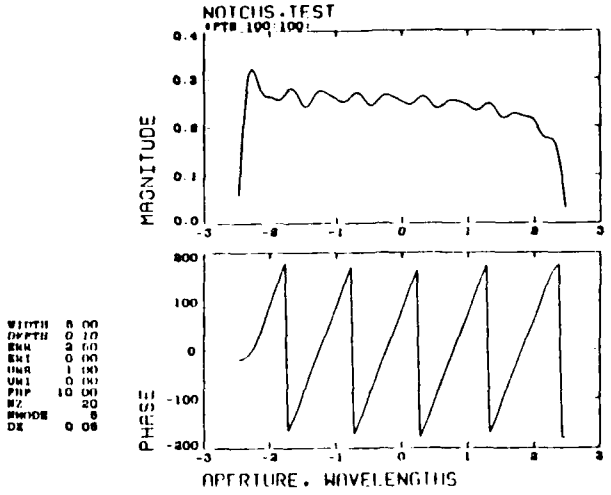

(a)

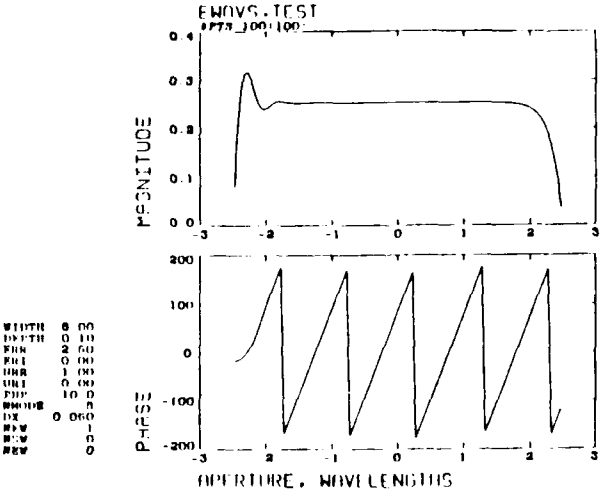

(b)

Figure 4.17. Current distribution in the aperture of a wide and shallow cavity for near grazing incidence.

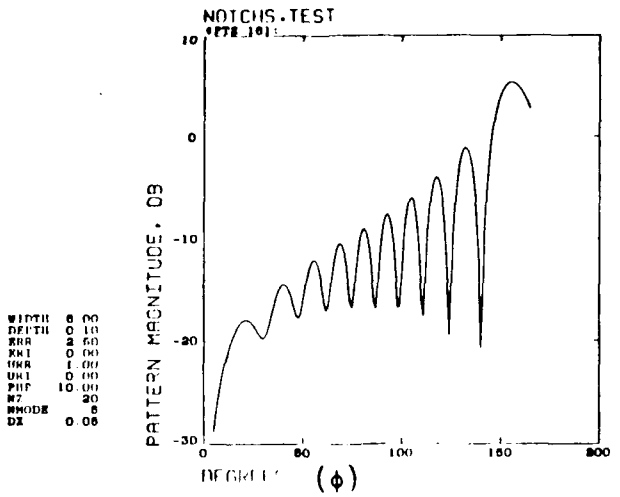

(a)

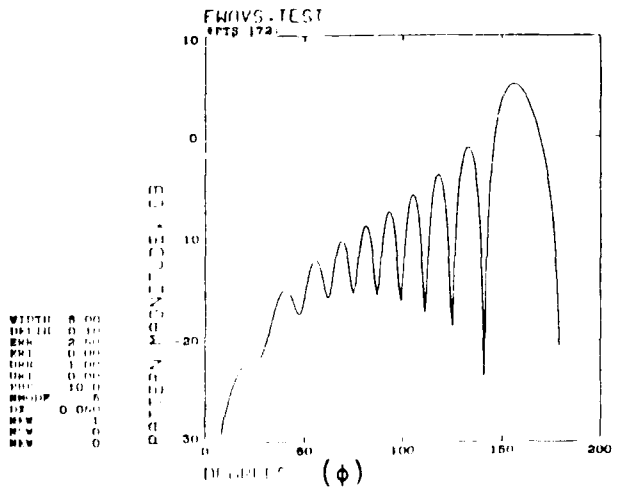

(b)

Figure 4.18. Bistatic scattering by a wide and shallow cavity for near grazing incidence.

Figures 4.19 to 4.22 show the monostatic scattered field results for cavities of depths .10λ, .15λ, .20λ and .25 λ. Inaccuracies in the grazing incidence region are plainly visible in Figures 4.19 and 4.20. Inclusion of a surface wave type of field in the hybrid solution for b=.15λ improved the solution which employed a forced wave only, especially for normal incidence. However, the grazing incidence solution was only slightly improved. The hybrid solutions for b=.20λ and .25λ employ a forced wave and true surface waves, since the dominant surface wave mode is no longer cutoff. Figures 4.21 and 4.22 show the poor agreement between the hybrid and modal basis solutions. Examination of the bistatic scattered field patterns for these geometries shows fairly good agreement for normal incidence, but very poor agreement for grazing incidence. Attempts to improve the hybrid solution by the use of transition terms occasionally yielded better results. However, as was true for the hard polarization, a consistently accurate set of basis functions was not found for the deeper cavities. In short, a fairly accurate and very efficient hybrid solution for the soft polarization was found for cavities with depths < .10λ and of arbitrary width.

An alternative hybrid scheme for both the hard and soft polarizations would be to use the proper transition functions associated with the phenomenon of edge diffraction within the surface wave transition region. Such functions, involving Fresnel integrals and terms of the type $\rho^{-3/2}$, could be determined from asymptotic study of an appropriate canonical problem. However, use of these transition

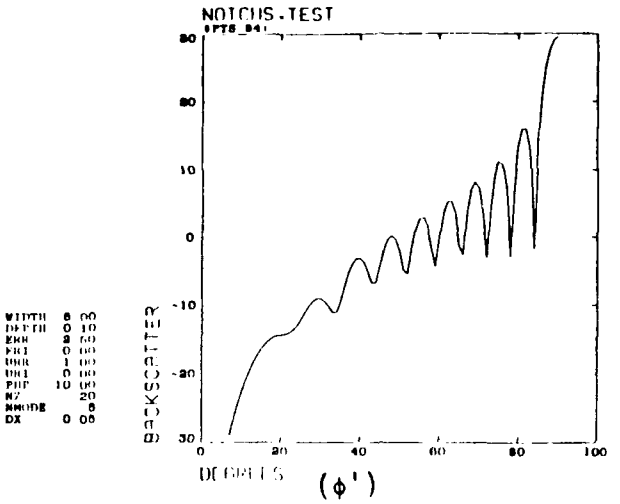

(a)

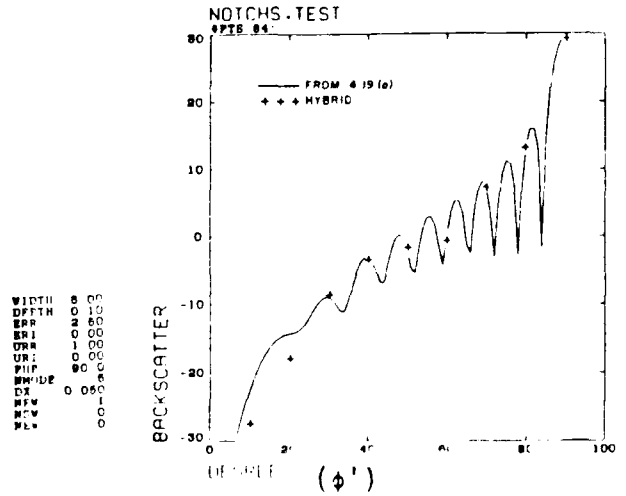

(b)

Figure 4.19. Backscattering by a wide and shallow cavity.

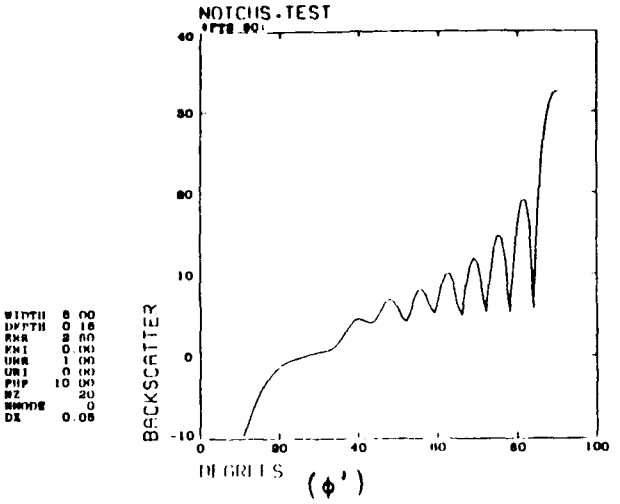

(a)

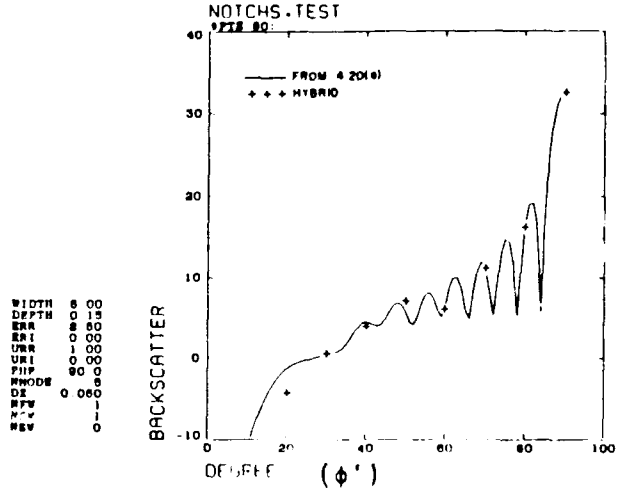

(b)

Figure 4.20. Backscattering by a wide and shallow cavity.

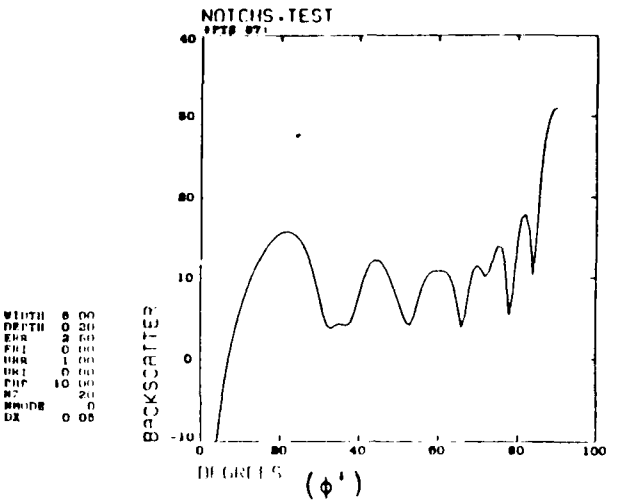

(a)

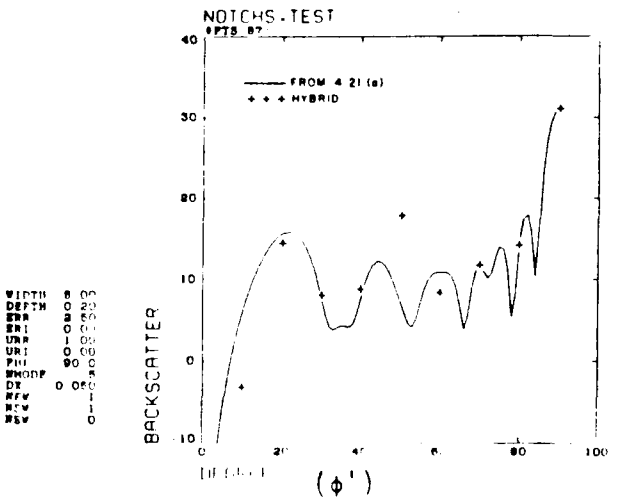

(b)

Figure 4.21. Backscattering from a wide and shalllow cavity.

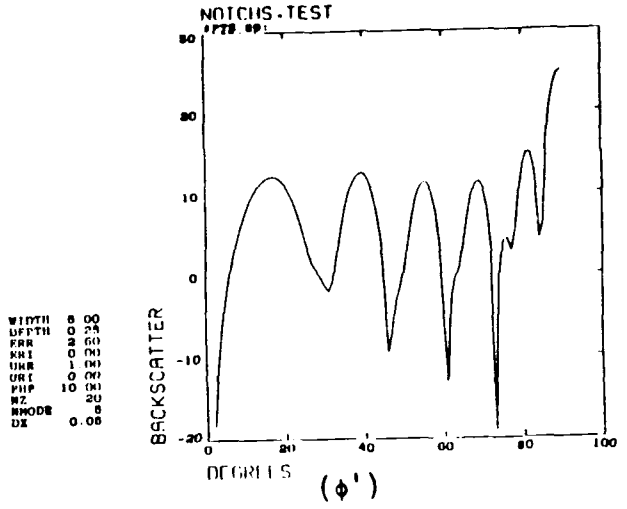

(a)

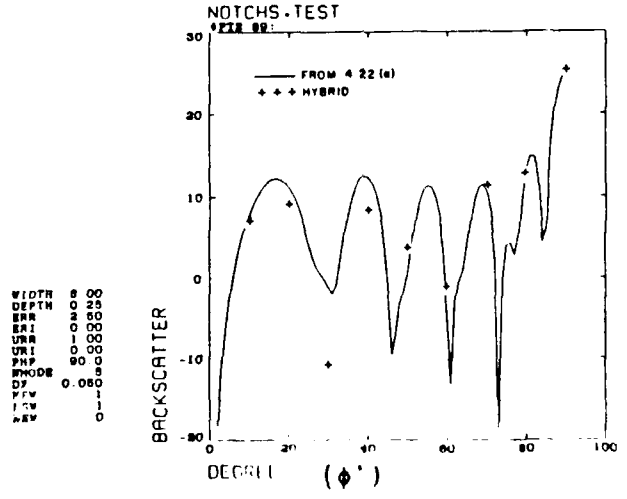

(b)

Figure 4.22. Backscattering from a wide and shallow cavity.

functions in a hybrid moment method solution would greatly increase the CPU required to compute the Z_{mn}, assuming Galerkin's method is employed. Use of point-matching may alleviate this problem.

Next, we consider the effects of loading on the scattering patterns of the wide shallow cavities. Comparisons will be made using only results from the modal basis solution. Considering first the hard polarization, Figures 4.23 through 4.27 show the backscattered field magnitude for a cavity of width=5λ and depth=.1λ and for various dielectric loading; in all cases μ_r=1. These figures should be compared with Figure 4.10 for which ε_r=2.5 and for which a significant surface wave is present. The backscatter of an unloaded cavity, shown in Figure 4.13, shows significantly less backscatter along grazing angles due to the lack of surface wave. A lossy dielectric, ε_r=2.5-j.25, is shown in Figure 4.24. Again the most significant differences compared to Figure 4.10 occur for grazing angles. Figure 4.25 is for a dielectric constant ε_r=5 and displays no significant differences in backscatter. However, Figures 4.26 and 4.27 are for larger dielectric constants, ε_r=10 and ε_r=15, respectively, and show a pronounced decrease in backscatter along grazing angles as compared with Figure 4.10. This effect is due to the destructive interference of surface wave reflections and will, therefore, vary with the cavity width.

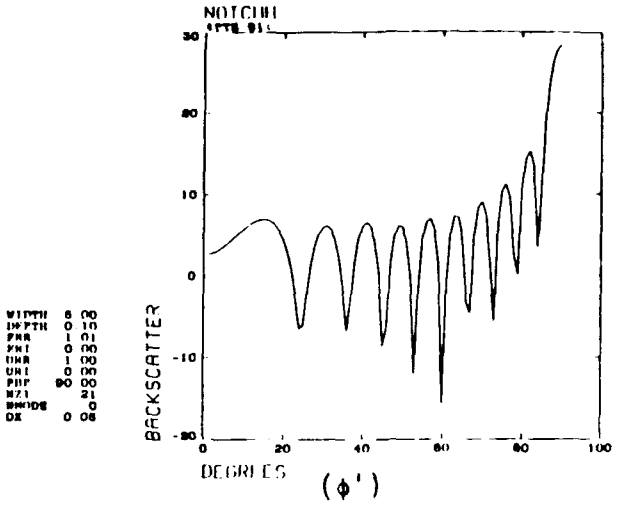

Figure 4.23. Backscattering from a wide and shallow cavity.

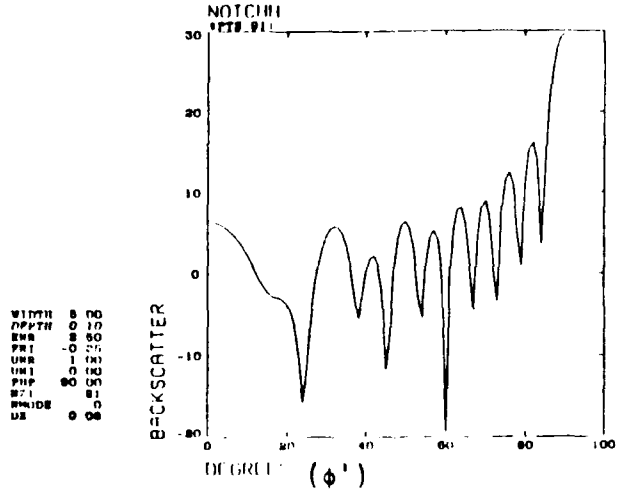

Figure 4.24. Backscattering from a wide and shallow cavity.

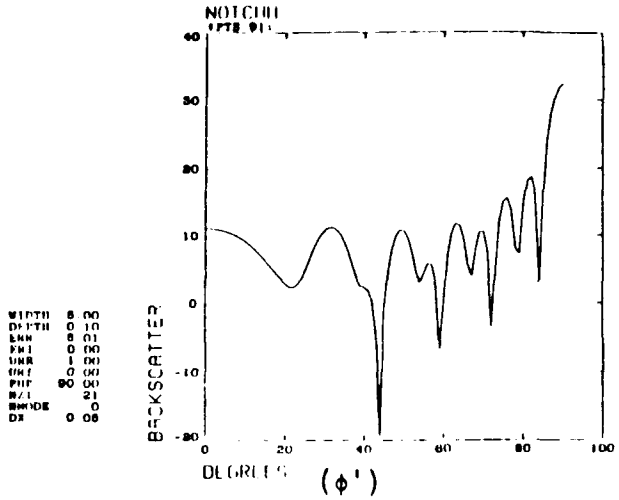

Figure 4.25. Backscattering from a wide and shallow cavity.

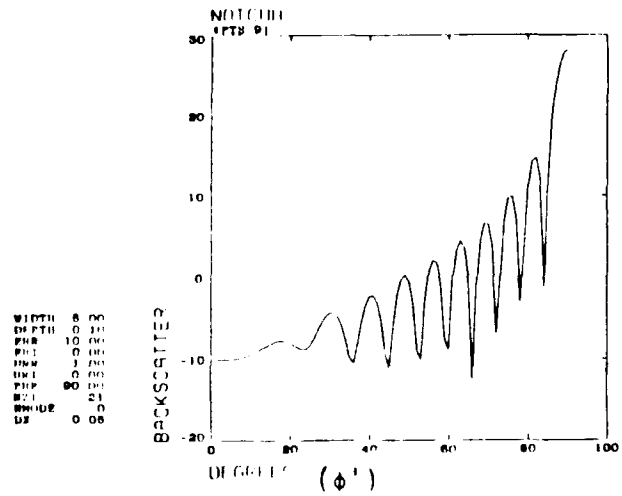

Figure 4.26. Backscattering from a wide and shallow cavity.

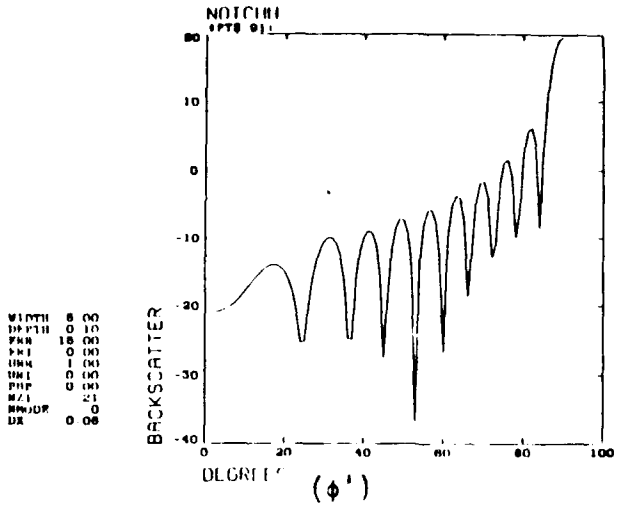

Figure 4.27. Backscattering from a wide and shallow cavity.

Figure 4.28 shows the backscatter from a cavity of width=9.5λ and depth=.25λ with a dielectric constant ε_r=2.5. This geometry is easily shown to be surface wave resonant (β_n=8.599 from Table 4.1); however, this is the case is readily apparent from the plot. Figure 4.29 dramatically displays the effect of adding loss to the dielectric, ε_r=2.5-j.25, thus removing the resonance by both altering the resonant frequency and damping the surface waves.

Consider now the effects of loading on the backscatter patterns for the soft polarization. Figures 4.30 through 4.34 are for a cavity of width=5λ and depth=.1λ and for various types of dielectric loading. These should be compared with Figure 4.19 for which ε_r=2.5 and for which

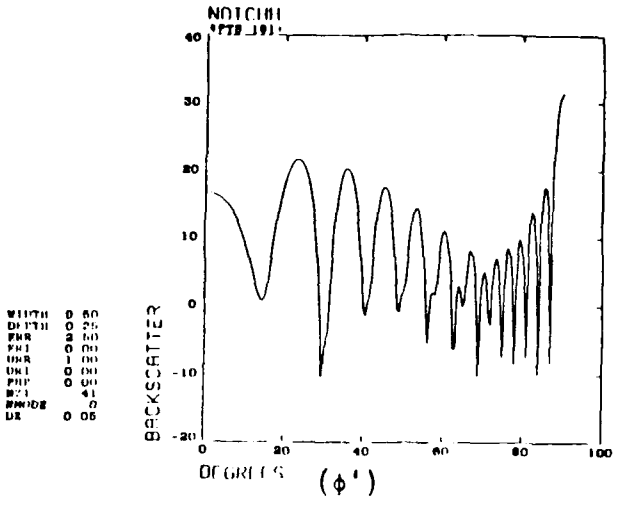

Figure 4.28. Backscattering from a wide and shallow cavity.

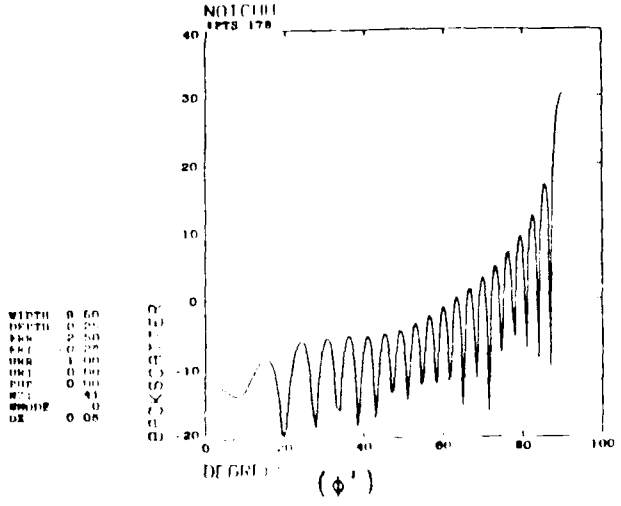

Figure 4.29. Backscattering from a wide and shallow cavity.

a significant surface wave is not present. Figures 4.30 and 4.31 show the backscatter of an unloaded cavity and of a cavity containing a lossy dielectric with ε_r=2.5-j.25, respectively. Neither of these show much difference when compared with Figure 4.19 simply because of the lack of surface wave in each case. The same rationale applies to Figure 4.32 for which ε_r=5, even though the surface wave is only slightly below cutoff. For Figure 4.33, for which ε_r=10, the surface wave mode (or modes) are above cutoff as is readily apparent from the backscatter pattern. Figure 4.34, for which ε_r=15, shows a decrease in backscatter compared with Figure 4.33 for near-grazing angles, although not nearly as pronounced as was observed for the hard polarization.

Figure 4.35 shows the backscatter from an unloaded cavity of width=5λ and depth=.25λ. Comparing this with Figure 4.22, for which ε_r=2.5 and for which a surface wave is present, the significance of the surface wave at grazing and near-grazing angles is readily apparent.

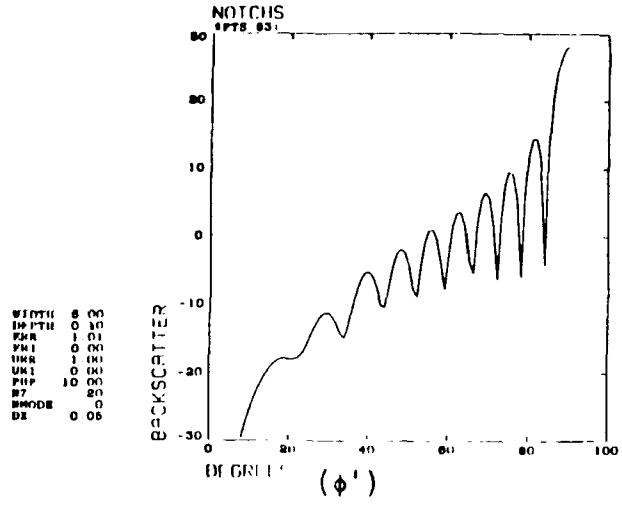

Figure 4.30. Backscattering from a wide and shallow cavity.

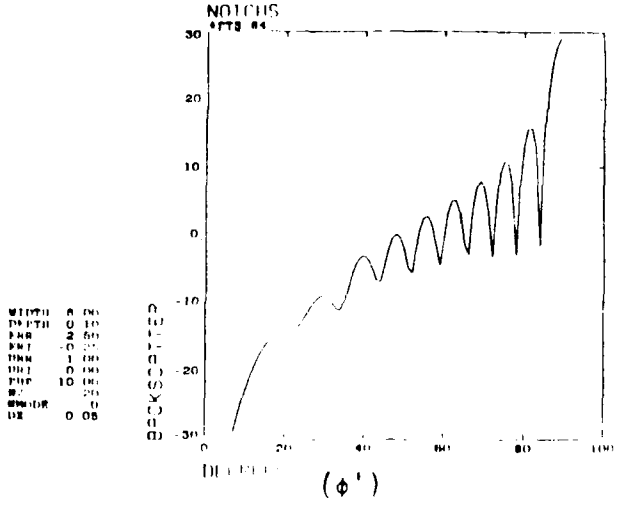

Figure 4.31. Backscattering from a wide and shallow cavity.

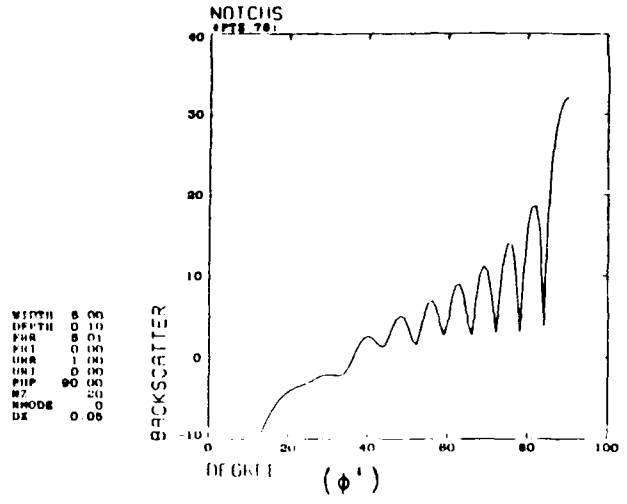

Figure 4.32. Backscattering from a wide and shallow cavity.

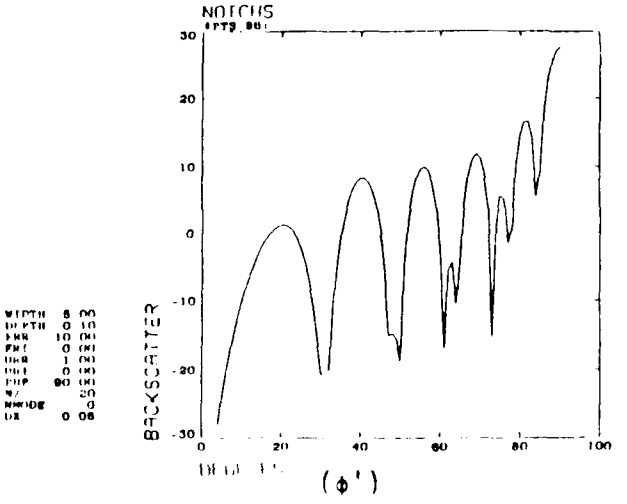

Figure 4.33. Backscattering from a wide and shallow cavity.

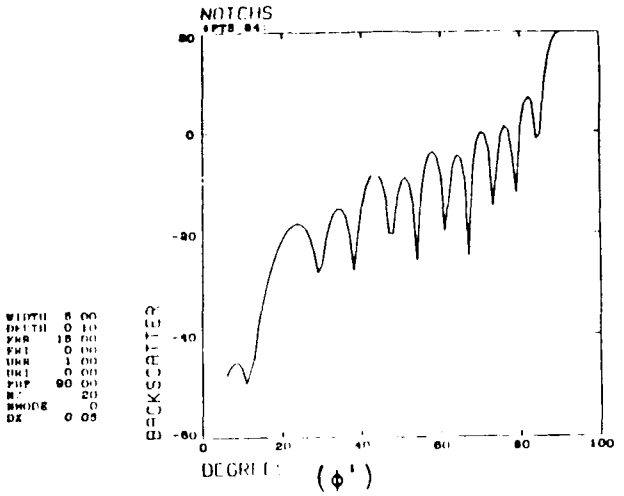

Figure 4.34. Backscattering from a wide and shallow cavity.

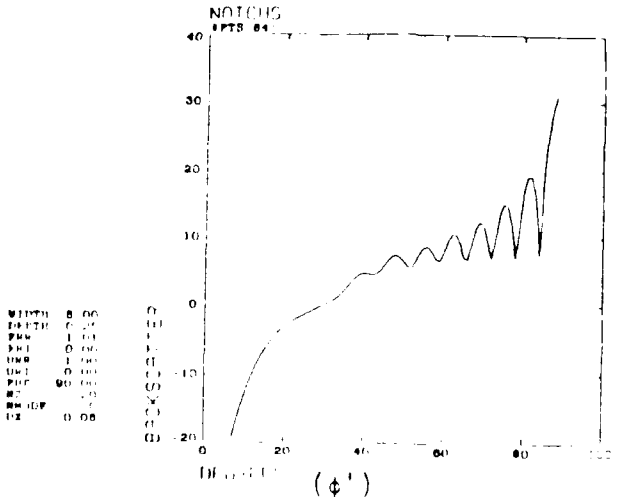

Figure 4.35. Backscattering from a wide and shallow cavity.

V. CONCLUSIONS

Two efficient moment method solutions have been developed for the scattering of an electromagnetic plane wave from a 2-D rectangular cavity recessed in a perfectly conducting ground plane and loaded with a homogeneous lossy or lossless dielectric. Integral equations for the equivalent magnetic current in the cavity aperture are solved by Galerkin's method for the hard and soft polarizations independently. One of the solutions termed a modal basis solution, expands the equivalent magnetic current in a set of parallel plate waveguide modes which constitute entire domain basis functions over the whole aperture. This solution requires 3-4 unknowns per aperture wavelength, versus 10-20 unknowns per wavelength when using pulses or piecewise sinusoids. In addition, a portion of the cavity Green's function contribution to the impedance matrix elements was summed into closed form resulting in a highly convergent representation. When compared with a pulses/point-matching solution for the hard polarization, the modal basis solution was found to be several times as efficient without loss of accuracy. At present, this solution is limited to geometries with aperture widths $\lesssim 25\lambda$ (requiring 75-100 unknowns) as a matter of computational efficiency; the required CPU is independent of cavity depth and loading.

A second moment method solution, termed a hybrid basis solution, was developed specifically for wide shallow cavities with enough loading to support at most one surface wave mode. The hybrid basis solution

employs entire basis functions and Galerkin's method, as does the modal basis solution, but expands the equivalent magnetic current as a sum of forced wave, two surface waves (if present) and several transition waves. The transition waves are exponential functions chosen to be most significant near the edges of the aperture in the surface wave transition region. This representation was found to yield accurate results for the hard polarization for cavity depths $\lesssim .10\lambda$ and widths $\gtrsim$ several λ with the use of just 3-4 transition waves. Thus, since only about 10 unknowns are required for any aperture width and the basis functions are not significantly more complicated than are the modal basis functions, the hybrid basis solution is an extremely efficient solution for wide shallow cavities. For the soft polarization the surface wave mode was not present for cavity depths $\lesssim .10\lambda$ and for the choice of dielectric material considered. Also, the transition waves were found to not be appropriate for this polarization. Thus, only the forced wave plus two exponentials, chosen so that the forced wave would meet the proper edge condition, made up the hybrid basis functions. Fairly accurate results were obtained for cavity depths $\lesssim .10\ \lambda$ and widths $\gtrsim$ several λ, except near grazing angles of incidence. Again, this hybrid basis solution is extremely efficient.

The analytical techniques presented here should prove useful in the design of surface wave antennas and in determining the RCS contribution from such structures as well as from loaded and unloaded notch structures. Future research could include modification to the cavity Green's function to accomodate, for example, impedance side walls.

Improvements to the hybrid basis solution, specifically, may be made by choosing more appropriate transition wave basis functions. Such basis functions may be obtained from a UTD analysis of an appropriate canonical surface wave diffraction problem, or perhaps by using many pulses or piecewise sinusoids near the edges of the aperture.

APPENDIX A

DERIVATION OF THE INTEGRAL EQUATIONS

The integral Equations (2.2) and (2.4) for the region I ($y>0$) and region II ($y<0$) fields, respectively, may be derived from Green's second identity for scalar fields and the equivalence theorem. In two dimensions Green's second identity has the form [16]

$$\int_L \left(\psi \frac{\partial \phi}{\partial n} - \phi \frac{\partial \psi}{\partial n}\right) d\ell = \iint_s (\psi \nabla^2 \phi - \phi \nabla^2 \psi)\, ds \qquad (A.1)$$

where ψ and ϕ are scalar fields and s is a surface bounded by the contour L. Note that this identity is a statement of reciprocity for the two fields.

Let ϕ be the scalar field, u^s_h, defined by

$$u^s_h(\bar{\rho}) = \begin{bmatrix} E_z(\bar{\rho}) \\ H_z(\bar{\rho}) \end{bmatrix}, \qquad (A.2)$$

and let ψ be the appropriate Green's function, $G^s_h(\bar{\rho},\bar{\rho}')$. To derive integral equations from (A.1) we must consider the wave equations and boundary conditions satisfied by u and G. The scalar fields satisfy

$$(\nabla^2 + k^2)\, u^s_h(\bar{\rho}) = \begin{bmatrix} j\omega\mu & J_z \\ j\omega\epsilon & M_z \end{bmatrix}, \qquad (A.3)$$

where J_z, M_z are impressed sources located in region I as shown in Figure A.1. On perfect conductors, i.e., paths L_c and C, the fields must satisfy the boundary conditions

$$\begin{bmatrix} u_s \big|_L \\ \frac{\partial u_h}{\partial n} \big|_L \end{bmatrix} = 0 \qquad (A.4)$$

where $L = L_c$ or C and $\hat{n}$ is the interior normal along L. The Green's function satisfies

$$(\nabla^2 + k^2)\, G_{\substack{s \\ h}}(\bar{\rho},\bar{\rho}') = -\delta(\bar{\rho},\bar{\rho}') \quad , \qquad (A.5)$$

with boundary conditions chosen so as to simplify (A.1) as much as possible.

To facilitate determination of the Green's function the original problem of Figure A.1 is converted into an equivalent problem by employing the equivalence principle. A perfectly conducting sheet is placed in the aperture, and on this sheet equivalent source distributions are placed on either side. Then, for the equivalent problem in region I, application of Green's identity along with Equations (A.3), (A.4) and (A.5) yields

$$\int_{L_a} \left(G_{\substack{s \\ h}}(\bar{\rho},\bar{\rho}') \frac{\partial u_{\substack{s \\ h}}}{\partial n}(\bar{\rho}') - u_{\substack{s \\ h}}(\bar{\rho}') \frac{\partial G_{\substack{s \\ h}}}{\partial n}(\bar{\rho},\bar{\rho}') \right) d\ell'$$

$$= \iint_{S_I} G_{\substack{s \\ h}}(\bar{\rho},\bar{\rho}') \begin{Bmatrix} j\omega\mu & J_o \\ j\omega\epsilon & M_o \end{Bmatrix} ds' + u_{\substack{s \\ h}}(\bar{\rho}) \qquad (A.6)$$

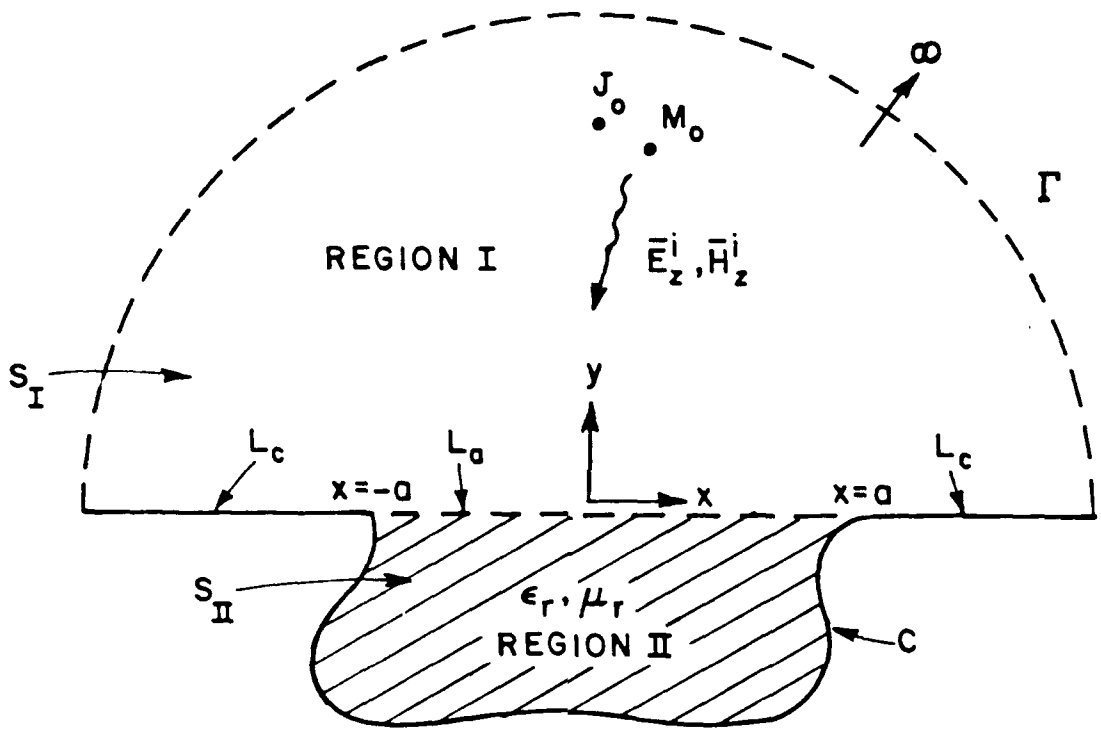

Figure A.1. Geometry for derivation of integral equations.

Choosing the boundary conditions

$$\left[\frac{\partial G_h}{\partial n}\right]_{G_s} = 0 \text{ on } L_a \quad , \tag{A.7}$$

G_{s_h} becomes the half-space Green's function

$$G_{s_h}(x,y;x',y') = -j/4\, H_o^{(2)}\left(k\sqrt{(x-x')^2 + (y-y')^2}\right)$$

$$\pm\, j/4\, H_o^{(2)}\left(k\sqrt{(x-x')^2 + (y+y')^2}\right) \tag{A.8}$$

Assume the sources in region I to be z-directed electric and magnetic line sources for the soft and hard polarizations, respectively, located at (x_o, y_o). Then from Figure A.1 and Equations (A.7) and (A.6), Equation (A.6) becomes

$$u_{s,h}(\bar{\rho}) = u^{i}_{s,h}(\bar{\rho}) + u^{r}_{s,h}(\bar{\rho}) \mp \int_{-a}^{a} \left| \begin{matrix} u_s(\bar{\rho}') \dfrac{\partial}{\partial y'} G_s(\bar{\rho},\bar{\rho}') \\ \dfrac{\partial u_h}{\partial y'}(\bar{\rho}')\, G_h(\bar{\rho},\bar{\rho}') \end{matrix} \right| \Bigg|_{y=0+} dx' \qquad (A.9)$$

where

$$u^{i}_{s,h}(\bar{\rho}) = \begin{Bmatrix} E_o \\ H_o \end{Bmatrix} H_o^{(2)}\left(k\sqrt{(x-x_o)^2 + (y-y_o)^2}\right) \qquad (A.10a)$$

$$u^{r}_{s,h}(\bar{\rho}) = \begin{Bmatrix} -E_o \\ H_o \end{Bmatrix} H_o^{(2)}\left(k\sqrt{(x-x_o)^2 + (y+y_o)^2}\right) \quad . \qquad (A.10b)$$

and where $u_{s,h}$ is given by Equation (A.8). In this work the incident field is assumed to be (locally) a plane wave, thus the asymptotic form of Equation (A.10) is used. This completes the derivation of the integral equation for the fields in region I.

For the equivalent problem in region II, application of Green's identity and Equations (A.4) and (A.5) (there are no sources in this region) yields

$$\int_{L_a} \left(G_{s,h}(\bar{\rho},\bar{\rho}') \frac{\partial u_{s,h}(\bar{\rho}')}{\partial n} - u_{s,h}(\bar{\rho}') \frac{\partial G_{s,h}}{\partial n}(\bar{\rho},\bar{\rho}') \right) d\ell'$$

$$= u_{s,h}(\bar{\rho}) \quad . \qquad (A.11)$$

Choosing the boundary conditions as given by Equation (A.7) $G_{\substack{s \\ h}}$ becomes the Green's functions for the enclosed cavity (derived in Appendix B). Applying the boundary conditions Equation (A.11) becomes

$$u_{\substack{s \\ h}}(\bar{\rho}) = \mp \int_{-a}^{a} \left[\begin{array}{l} u_s(\bar{\rho}') \frac{\partial}{\partial y'} G_s(\bar{\rho},\bar{\rho}') \\ \frac{\partial u_h}{\partial y'}(\bar{\rho}')\, G_h(\bar{\rho},\bar{\rho}') \end{array} \right]_{y'=0^-} dx \qquad (A.12)$$

Where $G_{\substack{s \\ h}}$ is the cavity Green's functions. This completes the derivation of the integral equation for the fields in region II.

APPENDIX B

DERIVATION OF THE CAVITY GREEN'S FUNCTIONS

The cavity Green's function for the geometry of Figure 2.3 is easily derived by the method of separation of variables. The Green's functions satisfy

$$\left(\frac{\partial^2}{\partial x^2} + \frac{\partial^2}{\partial y^2} + k^2\ \varepsilon_r\ \mu_r\right)\ G_{\substack{s\\h}}\ (x,y;x',y') = -\delta(x-x')\ \delta(y-y') \qquad (B.1)$$

with the boundary conditions

$$\left[\begin{array}{c} G_s \\ \dfrac{\partial G_h}{\partial n} \end{array}\right] = 0 \qquad \text{on } C \quad , \qquad (B.2)$$

where C is the perimeter of the cavity defined by x=-a, x=a, y=-b, y=0 and $\hat{n}$ is the interior normal on C. Consider the separation of variables [20]

$$G_{\substack{s\\h}}\ (x,y;x',y') = K\ X_{\substack{s\\h}}\ (x,x') \cdot Y_{\substack{s\\h}}\ (y,y') \quad , \qquad (B.3)$$

where K is a linear operator such that Equation (B.3) is a solution to Equation (B.1). Substituting (B.3) into (B.1) suggests the ordinary differential equations

$$\left(\frac{\partial^2}{\partial x^2} + \lambda_x\right)\ X_{\substack{s\\h}}\ (x,x') = -\delta(x-x') \qquad (B.4a)$$

$$\left(\frac{\partial^2}{\partial y^2} + \lambda_y\right)\ Y_{\substack{s\\h}}\ (y,y') = -\delta(y-y') \quad , \qquad (B.4b)$$

with the boundary conditions

$$\begin{vmatrix} X_s \\ \frac{dX_h}{dx} \end{vmatrix} = 0 \quad \text{on} \quad x=-a,\ x=a \tag{B.5a}$$

$$\begin{vmatrix} Y_s \\ \frac{dY_h}{dy} \end{vmatrix} = 0 \quad \text{on} \quad y=-b,\ y=0 \quad , \tag{B.5b}$$

and where

$$\lambda_x + \lambda_y = k^2\ \varepsilon_r\ \mu_r \tag{B.6}$$

Note that k is the free-space wavenumber.

Eigenfunction representations for X and Y are given by [21]

$$X(x,x';\ \lambda_x) = -\sum_m \frac{\phi_m(x)\ \phi_m(x')}{\lambda_x - \lambda_m} \tag{B.7a}$$

$$Y(y,y';\ \lambda_y) = -\sum_n \frac{\psi_n(y)\ \psi_n(y')}{\lambda_y - \lambda_n} \tag{B.7b}$$

where the $\{\phi_m(x)\}$, $\{\psi_n(y)\}$ are complete sets of orthonormal eigenfunctions arising from

$$\left(\frac{d^2}{dx^2} + \lambda_m\right)\ \phi_m(x) = 0 \tag{B.8a}$$

$$\left(\frac{d^2}{dy^2} + \lambda_n\right)\ \psi_n(y) = 0 \tag{B.8b}$$

and the appropriate boundary conditions. Consideration of the form of Equation (B.7) leads to the choice of linear operator

$$K = \kappa \int_{C_x} \dots \, d\lambda_x \tag{B.9a}$$

or

$$K = \kappa \int_{C_y} \dots \, d\lambda_y \tag{B.9b}$$

For this problem the constant κ is easily shown to be

$$\kappa = \frac{-1}{2\pi j} \tag{B.10}$$

Note that the paths of integration, C_x and C_y, encircle the singularities of X and Y, respectively. From Equations (B.7a) and (B.9a), Equation (B.3) can be shown to reduce to

$$G(x,y;x',y') = \sum_m \phi_m(x)\, \phi_m(x') \cdot Y(y,y';\lambda_m) \quad . \tag{B.11a}$$

If, instead, Equations (B.7b) and (B.9b) are used the result is

$$G(x,y;x',y') = \sum_n \psi_n(y)\, \psi_n(y') \cdot X(x,x';\lambda_n) \quad . \tag{B.11b}$$

Consider first the form of the Green's function given by Equation (B.11b). The orthonormal eigenfunctions arising from Equation (B.8b) with the boundary conditions

$$\begin{bmatrix} \psi_{s,\ell} \\ \dfrac{\partial \psi_{h,\ell}}{\partial y} \end{bmatrix} = 0 \quad \text{on} \quad y=-b,0 \tag{B.12}$$

are

$$\begin{bmatrix} \psi_{s,\ell}\,(y) \\ \psi_{h,\ell}\,(y) \end{bmatrix} = \begin{bmatrix} \sqrt{\dfrac{2}{b}} & \sin \dfrac{\ell\pi y}{b} \\ \sqrt{\dfrac{2}{b\epsilon_{\ell 0}}} & \cos \dfrac{\ell\pi y}{b} \end{bmatrix} \quad , \tag{B.13}$$

where ℓ is an integer and $\varepsilon_{\ell 0}$ is given by Equation (2.13c). In Equations (B.11b) $X(x,x')$ is determined from Equations (B.4a) and (B.6) with

$$\lambda_y = \frac{\ell^2\pi^2}{b^2} \quad . \tag{B.14}$$

The solution for $X(x,x')$ is constructed in two intervals and the properties of the Green's function at $x=x'$ are used to determine the arbitrary coefficients involved. That is,

$$X(x,x';\lambda_y) = \frac{U(x_<;\lambda_y) \cdot T(x_>;\lambda_y)}{W(T,U)} \tag{B.15}$$

where U and T are independent solutions of

$$\left(\frac{d^2}{dx^2} + \left(k^2\ \varepsilon_r\ \mu_r - \frac{\ell^2\pi^2}{b^2}\right)\right) \quad \begin{Bmatrix} U(x) \\ T(x) \end{Bmatrix} = 0 \tag{B.16}$$

and the constant W is (for Equation (B.16))

$$W(T,U) = T(x)\ U'(x) - T'(x) \cdot U(x) \quad . \tag{B.17}$$

Solutions to Equation (B.16) are

$$\begin{vmatrix} U_s(x) \\ T_s(x) \end{vmatrix} = \begin{vmatrix} \sin\gamma(a+x) \\ \sin\gamma(a-x) \end{vmatrix} \tag{B.18}$$

for the soft polarization and

$$\begin{vmatrix} U_h(x) \\ T_h(x) \end{vmatrix} = \begin{vmatrix} \cos\gamma(a+x) \\ \cos\gamma(a-x) \end{vmatrix} \tag{B.19}$$

for the hard polarization, where γ is given by Equations (2.13a) and (2.13b). The constant W is

$$W_{\substack{s \\ h}} = \pm \gamma \sin 2\gamma a \tag{B.20}$$

for the soft and hard polarizations, respectively. From Equations (B.18), (B.19) and (B.20), Equation (B.15) may be written in the form

$$X_{\substack{s \\ h}}(x,x') = \frac{-\csc 2\gamma a}{2\gamma}\left[\cos\gamma(2a-|x-x'|) \mp \cos\gamma(x+x')\right] \quad . \tag{B.21}$$

Finally, (B.11b), (B.13) and (B.21) yield the results given by Equations (2.12a) and (2.12b).

Consider now the form of the Green's function specified by Equation (B.11a). An orthonormal set of eigenfunctions is determined from Equation (B.8a) with appropriate boundary conditions. Equation (B.4b) is then solved by the same method used to solve Equation (B.4a) in the previous derivation. The final results for the Green's functions are

$$G_s(x,y;x',y') = \frac{-1}{2a}\sum_{\ell=1}^{\infty}\frac{\csc\gamma b}{\gamma}\sin\frac{\ell\pi}{2a}(a-x)\sin\frac{\ell\pi}{2a}(a-x')$$
$$\cdot\left[\cos\gamma(b-|y-y'|) - \cos\gamma(b+y+y')\right] \tag{B.22a}$$

$$G_h(x,y;x',y') = \frac{-1}{2a}\sum_{\ell=0}^{\infty}\frac{\csc\gamma b}{\varepsilon_{\ell o}\,\gamma}\cos\frac{\ell\pi}{2a}(a-x)\cos\frac{\ell\pi}{2a}(a-x')$$
$$\cdot\left[\cos\gamma(b-|y-y'|) + \cos\gamma(b+y+y')\right] \tag{B.22b}$$

where

$$\gamma = \begin{cases} \sqrt{k^2\,\varepsilon_r\,\mu_r - \left(\frac{\ell\pi}{2a}\right)^2} & , \quad \ell < \frac{2ak}{\pi}\,\mathrm{Re}\,(\varepsilon_r\,\mu_r) \qquad \text{(B.23a)} \\ -j\sqrt{\left(\frac{\ell\pi}{2a}\right)^2 - k^2\,\varepsilon_r\,\mu_r} & , \quad \ell > \frac{2ak}{\pi}\,\mathrm{Re}\,(\varepsilon_r\,\mu_r) \quad . \qquad \text{(B.23b)} \end{cases}$$

APPENDIX C

DERIVATION OF Z_{mn}

In this appendix we derive expressions for the elements of the impedance matrices of the solutions presented in this thesis. Consider first the hard polarization. From Equations (3.8) and (2.7), let

$$Z_{mn} = \int_{-a}^{a}\int_{-a}^{a} [j/2\, H_o^{(2)}(k|x-x'|) - \varepsilon_r\, G_h\,(x,x')]\, m(x')\, w(x)\, dx'dx \tag{C.1}$$

where $m=M_n$ and $w=W_m$ and G_h is given by Equation (2.12b). Now consider just the first term in Equation (C.1). Let

$$Z_u = \int_{-a}^{a}\int_{-a}^{a} j/2\, H_o^{(2)}(k|x-x'|)\, m(x')\, w(x)\, dx'dx \quad . \tag{C.2}$$

This expression may be reduced to a single integral over the Hankel function through the coordinate rotation (the so-called Popovich transformation)

$$u = \frac{x-x'}{\sqrt{2}} \tag{C.3a}$$

$$u' = \frac{x+x'}{\sqrt{2}} \quad . \tag{C.3b}$$

The resulting integral is

$$Z_u = \int_{-\sqrt{2a}}^{\sqrt{2a}}\int_{-\sqrt{2a}+|u|}^{\sqrt{2a}-|u|} j/2\, H_o^{(2)}(\sqrt{2}k|u|)\, m\left(\frac{u'-u}{\sqrt{2}}\right)\, w\left(\frac{u'+u}{\sqrt{2}}\right)\, du'du \tag{C.4}$$

From Equations (3.13) and (3.30) we see that the basis functions and weighting functions are simply exponentials. Thus, let

$$m(x') = e^{jfx'} \tag{C.5a}$$

$$w(x) = e^{jgx} \quad . \tag{C.5b}$$

Substituting Equations (C.5) into Equation (C.4) and evaluating the integral over u',

$$Z_u = 4j \int_0^a H_o^{(2)}(2ku) \cos(f-g)u \, \frac{\sin[(f+g)(a-u)]}{f+g} \, du \quad . \tag{C.6}$$

For ku near zero the small argument form of the Hankel function [17],

$$H_o^{(2)}(k\rho) \approx 1 - j \frac{2}{\pi} \ln \left(\frac{\gamma k\rho}{2}\right) \quad , \quad k\rho \to 0 \tag{C.7}$$

where $\gamma = 1.781$, is used so that the singularity at the origin may be integrated out. Substituting (C.7) into (C.6) for $u < .05$ yields the approximate result,

$$Z_u\Big|_0^{\Delta u} = 4j\cos\left[(f-g)\frac{\Delta u}{2}\right] \cdot \frac{\sin\left[(f+g)\left(a-\frac{\Delta u}{2}\right)\right]}{f+g} \cdot \left[1-j\frac{2}{\pi}\ln\left(\frac{\gamma k\Delta u}{e}\right)\right] \Delta u \quad . \tag{C.7.}$$

For ku large ($2ku>5$) the large argument form of the Hankel function, as given by Equation (2.8.1), is used to express most of Equation (C.6) in terms of the complex error function [17],

$$\text{erfz} = \frac{2}{\sqrt{\pi}} \int_0^z e^{-t^2} \, dt \quad , \tag{C.8}$$

by employing the relations

$$\int \frac{e^{-\gamma x}}{\sqrt{x}}\, dx = \sqrt{\pi/\gamma}\ \operatorname{erf}\sqrt{\gamma x} \quad . \tag{C.9a}$$

$$\int \sqrt{x}\, e^{-\gamma x} dx = \sqrt{\pi/\gamma}\ \frac{\operatorname{erf}\sqrt{\gamma x}}{2\gamma} - \frac{\sqrt{x}\, e^{-\gamma x}}{\gamma} \quad . \tag{C.9b}$$

For $f+g \neq 0$ the relevant portion of Equation (C.6) becomes

$$Z_u\Big|_{0.4}^{a} = \frac{1}{f+g}\sqrt{\frac{j}{\pi k}} \cdot \left[e^{j(f+g)a} \int_{0.4}^{a} \frac{e^{-j2ku}}{\sqrt{u}} \cdot \left(e^{-j2fu} + e^{-j2gu}\right) du \right.$$

$$\left. -e^{-j(f+g)a} \int_{0.4}^{a} \frac{e^{-j2ku}}{\sqrt{u}} \cdot \left(e^{j2fu} + e^{j2gu}\right) du \right] , \tag{C.10}$$

which is easily evaluated with Equation (C.9a). For $f+g=0$ the corresponding result is

$$Z_u\Big|_{0.4}^{a} = 2j\sqrt{\frac{j}{\pi k}} \int_{0.4}^{a} (a-u)\, \frac{e^{-j2ku}}{\sqrt{u}} \cdot \left(e^{j(f-g)u} + e^{-j(f-g)u}\right) du \ , \tag{C.11}$$

which is easily evaluated with Equations (C.9a) and (C.9b). The remaining portion of the integration in Equation (C.6), from u=.05 to u=0.40, is evaluated numerically by the trapezoidal rule.

Efficient code for computation of the Hankel function and complex error function, as well as an efficient program for complex matrix inversion, were provided by Prof. J.H. Richmond. These routines are discussed in [12].

Next we consider the second term in Equation (C.1.), denoted Z_L, where

$$Z_L = -\varepsilon_r \int_{-a}^{a} \int_{-a}^{a} G_h(x,x')\, m(x')\, w(x)\, dx'dx \quad . \tag{C.12}$$

Substituting Equations (C.5a), (C.5b) and (2.12b) evaluated at $y=y'=0$ into Equation (C.12), the resulting double integral may be evaluated in a straight forward manner. The resulting sum is

$$Z_L = 4\frac{\varepsilon_r}{h}\,\frac{\sin(f+g)a}{f+g}\sum_{\ell=0}^{\infty}\frac{1}{\varepsilon_{\ell o}}\cdot\frac{1}{\gamma^2-f^2}$$

$$- 4\,\varepsilon_r \sum_{\ell=0}^{\infty}\frac{\csc 2\gamma a}{\varepsilon_{\ell o}\gamma}\,\frac{1}{\gamma^2-f^2}\left|\begin{matrix}-\\ \\ -\end{matrix}\right. \sin(\gamma+f)a\,\frac{\sin(\gamma+g)a}{\gamma+g}$$

$$\left.\begin{matrix}\\ \\ \end{matrix}\right| - \sin(\gamma-f)a\,\frac{\sin(\gamma-g)a}{\gamma-g}\left.\begin{matrix}-\\ \\ -\end{matrix}\right| \tag{C.13}$$

where γ is a function of ℓ and is given by Equation (2.13). The first sum in this expression may be put in closed form through the use of the relation [22]

$$\sum_{\ell=1}^{\infty}\frac{1}{\ell^2-\alpha^2} = \frac{1}{2\alpha^2} - \frac{\pi}{2\alpha}\cot\pi\alpha \quad . \tag{C.14}$$

Thus, the first sum in (C.13) becomes

$$\sum_{\ell=1}^{\infty}\frac{1}{\varepsilon_{\ell o}}\cdot\frac{1}{\gamma^2-f^2} = \frac{b}{2}\,\frac{\cot\left(b\sqrt{k^2\varepsilon_r\mu_r-f^2}\right)}{\sqrt{k^2\varepsilon_r\mu_r-f^2}} \quad . \tag{C.15}$$

For the cavity depths of interest in this work (< 1/4 wavelength) only a few terms of the second sum in Equation (C.13) are needed for

convergence, regardless of cavity width. Thus, with the use of Equation (C.15) a highly convergent formulation of Z_L has been achieved.

An equivalent expression for Z_L may be obtained by using the alternative form of the cavity Green's function given by Equation (B.22b). Substituting this expression evaluated at y=y'=0, along with Equations (C.5a) and (C.5b), into (C.12) yields the result

$$Z_L = \frac{\varepsilon_r}{a} \sum_{\ell=0}^{\infty} \frac{\cot\gamma b}{\varepsilon_{\ell o}\,\gamma} \cdot \left[\frac{\sin(f+p)a}{f+p} \cdot \left[(-1)^{\ell} \frac{\sin(g+p)a}{g+p} + \frac{\sin(g-p)a}{g-p} \right] + \frac{\sin(f-p)a}{f-p} \left[\frac{\sin(g+p)a}{g+p} + (-1)^{\ell} \frac{\sin(g-p)a}{g-p} \right] \right] \tag{C.16}$$

where γ is given by Equation (B.23) and

$$p = \frac{\ell\pi}{2a} \tag{C.17}$$

No convenient method was found for reducing any portion of the sum in Equation (C.16) to closed form, making this representation of Z_L far less convergent. The number of terms required in the summation is directly proportional to the width, and is typically equal to 10-15 times the width in wavelengths.

Now consider the soft polarization. In view of Equations (3.8) and (2.8) let

$$Z_u = \frac{j}{2} \int_{-a}^{a} \int_{-a}^{a} \frac{\partial^2}{\partial y^2} H_o^{(2)}\left(k\sqrt{(x-x')^2+y^2}\right) \Big|_{y\,=\,0^+} m(x')\, w(x)\, dx'dx \tag{C.18}$$

where $m(x')$ and $w(x)$ are basis and weighting functions such that

$$\begin{vmatrix} \bar{m}\ (\pm a) & \bar{} \\ \underline{w}\ (\pm a) & \underline{} \end{vmatrix} = 0 \quad . \qquad \begin{matrix} (C.19a) \\ (C.19b) \end{matrix}$$

From the differential equation which the 2-D half-space Green's function satisfies, and noting that $y \neq y'$, we obtain the relation

$$\frac{\partial^2}{\partial y^2} H_o^{(2)} (k|\bar{\rho}-\bar{\rho}'|) = -\left(\frac{\partial^2}{\partial x^2} + k^2\right) H_o^{(2)} (k|\bar{\rho}-\bar{\rho}'|) \qquad (C.20)$$

where $|\bar{\rho}-\bar{\rho}'|$ is given by Equation (2.3). Substituting this into Equation (C.18) we then integrate by parts to remove the derivatives on the Hankel function. The end-point terms reslting from this integration can be shown to vanish from a consideration of the ege condition and the small argument of the Hankel function, as given by Equations (2.14) and (C.7), respectively, and from the relation

$$\lim_{x \to 0} x^t \ell nx = 0 \quad , t > 0 \quad . \qquad (C.21)$$

The resulting form of Z_u is

$$Z_u = -k^2 \frac{j}{2} \int_{-a}^{a} \int_{-a}^{a} H_o^{(2)}(k|x-x'|)\ m(x')\ w(x)\ dx'dx$$

$$+ \frac{j}{2} \int_{-a}^{a} \int_{-a}^{a} H_o^{(2)}(k|x-x'|) \frac{\partial m}{\partial x'}(x') \frac{\partial w}{\partial x}(x)\ dx'dx \quad . \qquad (C.22)$$

From Equations (3.15) and (3.22) it is apparent that the basis and weighting functions are a sum of exponentials. Thus, the evaluation of Z_u for the soft polarization is fundamentally the same as for the hard polarization.

Finally, consider the second term in Equation (2.8). Let

$$Z_L = \frac{1}{\mu r} \int_{-a}^{a} \int_{-a}^{a} \left[\frac{\partial^2}{\partial y \partial y'} G_s(x,y;x',y')\right] \Big|_{\substack{y'=0^- \\ y=0^{--}}} m(x')w(x)dx'dx \qquad (C.23)$$

where $m(x')$ and $w(x)$ satisfy Equation (C.19). Substituting Equation (2.2) into (C.23) yields

$$Z_L = \frac{\pi^2}{\mu_r b^3} \sum_{\ell=1}^{\infty} \frac{\csc 2\gamma a}{\gamma} \ell^2 \cos \frac{\ell\pi y}{b} \cos \frac{\ell\pi y'}{b} \cdot I \qquad (C.24)$$

where

$$I = \int_{-a}^{a} \int_{-a}^{a} \left[\cos\gamma(2a-|x-x'|) - \cos\gamma(x+x')\right] m(x')w(x)\, dx'dx \qquad (C.25)$$

and γ is a function of ℓ as given by Equation (2.13). To obtain a convergent summation Equation (C.25) must be integrated by parts, which yields the result

$$I = \frac{1}{\gamma^2} \int_{-a}^{a} \int_{-a}^{a} \left[\cos\gamma(2a-|x-x'|) + \cos\gamma(x+x')\right] \frac{\partial m(x')}{\partial x} \frac{\partial w(x)}{\partial x} dx'dx$$

$$+ \frac{2\sin 2\gamma a}{\gamma} \int_{-a}^{a} m(x)w(x)\, dx \quad . \qquad (C.26)$$

Reecalling that $m(x')$ and $w(x)$ are a sum of exponentials for this polarization, we substitute Equations (C.5) into Equation (C.26) and evaluate the integrals in a straightforward manner. Employing the relation

$$\sum_{\ell=0}^{\infty} \frac{1}{\epsilon_{\ell o}\, b} \cos \frac{\ell\pi y}{b} \cos \frac{\ell\pi y'}{b} = \delta(y-y') \qquad (C.27)$$

along with Equation (C.14), and noting that $y \neq y'$, Equation (C.24) becomes

$$Z_L = Z_L^o - 4\pi^2 \frac{f^2 g}{\mu_r b^3} \sum_{\ell=1}^{\infty} \ell^2 \frac{\csc 2\gamma a}{\gamma^3} \frac{1}{\gamma^2 - f^2} \cdot \frac{1}{\gamma^2 - g^2}$$

$$\cdot \left[\sin(\gamma+f)a \frac{\sin(\gamma+g)a}{\gamma+g} - \sin(\gamma-f)a \frac{\sin(\gamma-g)a}{\gamma-g} \right] \quad , \qquad (C.28)$$

where

$$Z_L^o = \frac{2}{\mu_r} \frac{\sin(f+g)a}{f+g} \cdot \left[\frac{g}{f} \sqrt{k^2 \epsilon_r \mu_r - f^2} \right.$$

$$\left. \cdot \cot b \sqrt{k^2 \epsilon_r \mu_r - f^2} - \left(1 + \frac{g}{f} \sqrt{k^2 \epsilon_r \mu_r} \cot b \sqrt{k^2 \epsilon_r \mu_r}\right) \right] \qquad (C.29)$$

A second form for Z_L is obtained by employing the alternative form of the cavity Green's function given by Equation (B.22b). Substituting this expression into Equation (C.23) and noting that $y \neq y'$, Z_L becomes

$$Z_L = \frac{-1}{a} \sum_{\ell=1}^{\infty} \gamma \cot \gamma b \cdot I \quad , \qquad (C.30)$$

where

$$I = \int_{-a}^{a} \int_{-a}^{a} \sin p(a-x') \sin p(a-x) \, m(x') \, w(x) \, dx'dx \qquad (C.31)$$

and p is given by Equation (C.17). Integrating by parts, (C.31) becomes

$$I = \frac{1}{p^2} \int_{-a}^{a} \int_{-a}^{a} \cos p(a-x') \cos p(a-x) \frac{\partial m(x')}{\partial x'} \frac{\partial w(x)}{\partial x} \, dx'dx \quad . \qquad (C.32)$$

Substituting Equations (C.5) into (C.33) and evaluating the double integrals, Equation (C.32) is substituted into (C.30) and Z_L becomes

$$Z_L = \frac{fg}{\mu_r a} \sum_{\ell=1}^{\infty} \frac{\gamma \cot \gamma b}{p^2} \left[\frac{\sin(f+p)a}{f+p} \cdot \left[(-1)^{\ell} \frac{\sin(g+p)a}{g+p} + \frac{\sin(g-p)a}{g-p} \right] + \frac{\sin(f-p)a}{f-p} \left[\frac{\sin(g+p)a}{g+p} + (-1)^{\ell} \frac{\sin(g-p)a}{g-p} \right] \right], \quad \text{(C.33)}$$

where γ is given by Equation (B.23) and p is given by Equation (C.17).

Equations (C.28) and (C.33) possess the same convergance properties that the corresponding hard polarization equations have. Thus, Equations (C.28) and (C.29) yield a far more convergent representation than does Equation (C.33) for wide cavities.

REFERENCES

[1] R.F. Harrington, Field Computation by Moment Methods, MacMillan, New York, 1968.

[2] J.H. Richmond and M.C. Gilreath, "Flush-Mounted Dielectric-Loaded Axial Slot on a Circular Cylinder," IEEE Trans. on Antennas and Propagation, Vol. 75, pp. 348-351, May 1975.

[3] R. Kautz, P.H. Pathak and L. Peters, Jr., "EM Scattering by Slits and Grooves in Thick Perfectly-Conducting Planar Surfaces," Technical Report No. 714614-5, The Ohio State University, ElectroScience Laboratory, Columbus, Ohio, August 1984.

[4] N. Wang, "Electromagnetic Scattering from a Filled Slit in a Thick Conducting Screen, TM Case," Report 714349-8, The Ohio State University ElectroScience Laboratory, Dept. of Electrical Engineering, May 1984.

[5] P.H. Pathak and R.G. Kouyoumjian, "Surface Wave Diffraction by a Truncated Dielectric Slab Recessed in a Perfectly Conducting Surface," Radio Science, Vol. 14, pp. 405-417, 1979.

[6] J.B. Keller, "Geometrical Theory of Diffraction," J. Opt. Soc. Amer., Vol. 52, pp. 116-130, 1962.

[7] J. Pace and R. Mittra, "Generalized Scattering Matrix Analysis of Waveguide Discontinuity Problems," in Quasi-Optics, Vol. XIV, pp. 177-197, Polytechnic Institute of Brooklyn Press, New York, 1964.

[8] B. Noble, Methods Based on the Wiener-Hopf Technique, Pergamon, New York, 1958.

[9] C.W. Chuang, "Surface Wave Diffraction by a Truncated Inhomogeneous Dielectric Slab Recessed in a Perfectly Conducting Surface," IEEE Trans. on Antennas and Propagation, Vol. AP-34, No. 4, April 1986.

[10] G.A. Thiele and T.H. Newhouse, "A Hybrid Technique for Combining Moment Methods with the Geometrical Theory of Diffraction," IEEE Trans. on Antennas and Propagation Vol. AP-23, No. 1, Jan. 1975.

[11] W.D. Burnside, C.L. Yu, and R.J. Marhefka, "A Technique to Combine the Geometrical Theory of Diffraction and the Moment Method," IEEE Trans. on Antennas and Propagation Vol. AP-23, pp. 551-558, July 1975.

[12] J.H. Richmond, "Scattering by Thin Dielectric Strips," IEEE Trans. on Antennas and Propagation, pp. 64-68, January 1985.

[13] S. Srikanth, P.H. Pathak, and C.W. Chuang, "Hybrid UTD-MM Analysis of the Scattering by a Perfectly Conducting Semicircular Cylinder," IEEE Trans. on Antennas and Propagation, Vol. AP-34, No. 10, October 1986.

[14] R.G. Kouyoumjian and P.H. Pathak, "A Uniform Geometrical Theory of Diffraction for an Edge in a Perfectly Conducting Surface," IEEE Trans. on Antennas and Propagation, Vol. 62, pp. 1448-1461, Nov. 1974.

[15] P.H. Pathak and R.G. Kouyoumjian, "An Analysis of the Radiation from Apertures in Curved Surfaces by the Geometrical Theory of Diffraction," IEEE Trans. on Antennas and Propagation, Vol. 62, pp. 1438-1447, November 1974.

[16] R.F. Harrington, Time-Harmonic Electromagnetic Fields, McGraw-Hill Book Company, 1961.

[17] M. Abramowitz and I.A. Stegun, Handbook of Mathematical Functions, National Bureau of Standards, 1964.

[18] R.A. Hurd, "The Edge Condition in Electromagnetics," IEEE Trans. on Antennas and Propagation, Vol. 76, pp. 70-73, Nov. 1976.

[19] C.H. Walter, Traveling Wave Antennas, McGraw-Hill, New York, 1965.

[20] E.C. Titchmarsh, Theory of Functions, 2nd Ed., Oxford University Press, 1939.

[21] J.D. Jackson, Classical Electrodynamics, 2nd Edition, Wiley Eastern Limited, New Delhi, 1978.

[22] A. Papoulis, Signal Analysis, McGraw-Hill, 1977.